

Article

Genesis of Gabbroic Hosted Copper Mineralisations in the Albanian Mirdita Zone (Kçira, Thirra)

Anikó Vácz-Lovász ^{1,*}, Zoltán Kovács ^{2,3}  and Gabriella B. Kiss ¹ 

¹ Department of Mineralogy, Institute of Geography and Earth Sciences, Faculty of Sciences, ELTE Eötvös Loránd University, 1117 Budapest, Hungary; gabriella.b.kiss@ttk.elte.hu

² Lithosphere Fluid Research Lab, Department of Petrology and Geochemistry, ELTE Eötvös Loránd University, 1117 Budapest, Hungary; kozraat@gmail.com

³ Centre for Energy Research, Hungarian Research Network, 1122 Budapest, Hungary

* Correspondence: lovaszani@staff.elte.hu

Abstract: There is a wide variety of ore deposits in Albania, where 20% of the Cu resources belong to a deposit type of unknown genesis (sulphide-bearing quartz veins in gabbroic rocks). The focus of this paper is on two mineralisations of this type (Kçira and Thirra) in the Mirdita Zone, an ophiolite zone representing the Mesozoic Neotethys Ocean in the Dinarides. Our aim is to understand the ore-forming processes and the genesis of these deposits, which can be used in future exploration projects. According to the petrographical analysis, the host rock suffered propylitic alteration or subgreenschist facies metamorphism. Mineral chemistry of pyrite and epidote suggests a VMS related origin, more precisely, the deeper part of its stockwork feeder zone. The bulk rock geochemical analyses confirms that the mineralisations are classified as mafic-, Cyprus-type VMS deposits. Differences in the geochemical compositions and the corresponding mineralogical observations are attributed to the distinct original geotectonic positions: higher amount of compatible elements (Cr, Ni, V and Cu) occur in Kçira, which formed in a mid-oceanic ridge environment, while incompatible elements (Ag, As, Co and Zn) are more abundant in the Thirra deposit, which formed in a supra-subduction zone setting.



Citation: Vácz-Lovász, A.; Kovács, Z.; Kiss, G.B. Genesis of Gabbroic Hosted Copper Mineralisations in the Albanian Mirdita Zone (Kçira, Thirra).

Minerals **2024**, *14*, 195. <https://doi.org/10.3390/min14020195>

Academic Editor: Georgy Cherkashov

Received: 20 December 2023

Revised: 1 February 2024

Accepted: 8 February 2024

Published: 13 February 2024



Copyright: © 2024 by the authors. Licensee MDPI, Basel, Switzerland. This article is an open access article distributed under the terms and conditions of the Creative Commons Attribution (CC BY) license (<https://creativecommons.org/licenses/by/4.0/>).

1. Introduction

The majority of Albania's copper resources is related to the Mirdita Zone, which is part of the Dinaric ophiolite suite, representing the remnants of the Jurassic ocean floor of the Neotethys Ocean. These deposits represent three types of mineralisations: VMS deposits, volcanogenic-sedimentary Cu deposits, and gabbro hosted vein-type Cu-deposits (e.g., [1,2]).

The exploration and exploitation for copper is reviving in Albania, and numerous international companies have projects there. Though most of the Cu mineralisations belong to the VMS type, 20% of the country's Cu resources belong to a deposit type of unknown genesis [3]. This type of ore mineralisation occurs in the gabbroic units of the ophiolite series and is composed of pyrite, chalcopyrite, and pyrrhotite with quartz as the main gangue mineral. Width of the veins ranges from a few centimetres to twenty metres and their length from a few metres to a few hundred metres [4,5]. According to analogies, this gabbro hosted sulphide-bearing quartz mineralisation (formerly called quartz-sulphide veins, by [4]) could be generated either by regional metamorphic or by subseafloor hydrothermal processes. While the former type is scarce (found e.g., in Canada, Australia, Morocco or Slovakia) [6–9], the latter, submarine volcanism-related hydrothermal type is relatively common (e.g., Italy, Cyprus, Turkey, Oman). However, gabbro, as the host rock of the stockwork feeder zone, is relatively rare [10,11].

Therefore, we selected deposits of this peculiar type for investigation; they have not yet been examined with modern analytical methods, even though detailed descriptions of mineralisation with the definition of the deposit type have obvious importance in mineral exploration. Hence, this paper presents the petrographical, mineralogical, and textural analysis, together with the evaluation of the formation processes, using a wide range of analytical methods (X-ray Powder Diffraction—XRPD, scanning electron microscope—SEM, electron microprobe—EPMA, inductively coupled plasma optical emission spectrometry—ICP OES). However, the presented results bear not only regional geological importance, but contribute significantly to our knowledge on this uncommon deposit type. Our model can be used in the future to better understand similar gabbro-hosted VMS deposits in the Neotethyan belt and worldwide.

2. Geological Setting

Three main units can be distinguished in the orogeny of the Dinarides-Hellenides on the Balkan Peninsula: Inner Dinarides, External Dinarides, and the Dinaridic Ophiolite Belt in between. The Mesozoic Mirdita Zone is part of the Dinaridic Ophiolite Belt, outcropping on 4000 km² in Albania and representing the suture between two continental units, Apulia in the west and Korabi-Pelagonia in the east (Figures 1 and 2), e.g., [12,13]. The remnants of the Middle Jurassic Mirdita-Pindos oceanic basement crop out along this belt.

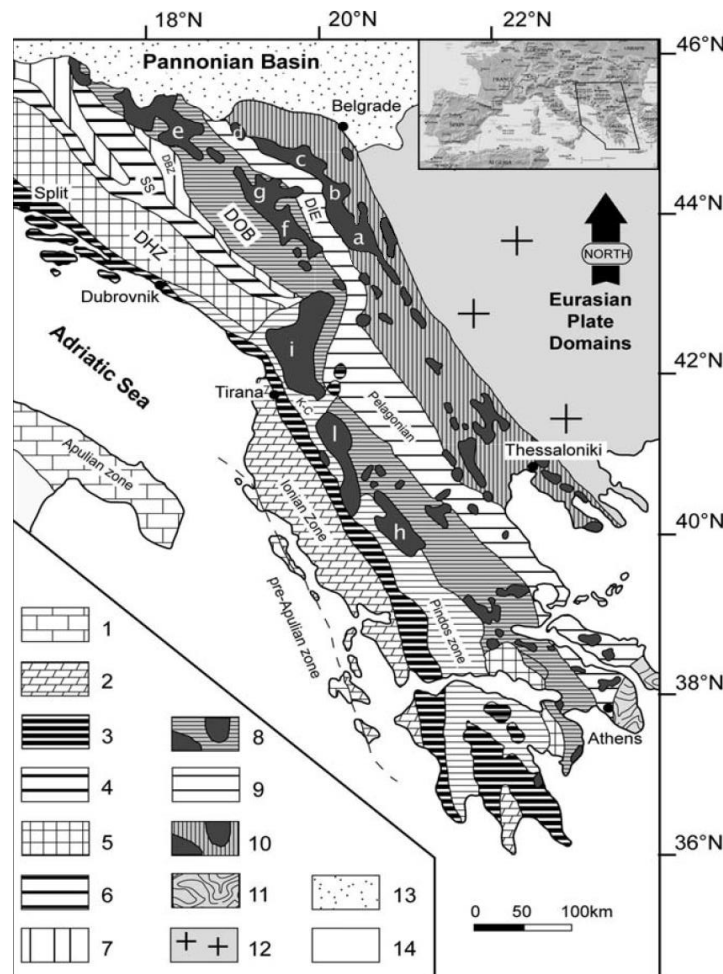


Figure 1. Simplified geological map of the Dinaric-Hellenic Belt, highlighting the major tectonic units, after [14]. Legend and abbreviations: 1—Apulian and Pre-Apulian Units; 2—Ionian Units; 3—South Adriatic Units: Kruja, Gavrovo and Tripolitsa; 4—Budva, Krasta-Cukali (K-C) and Pindos Units; 5—Dalmatian-Herzegovian (DHZ) Units; 6—Sarajevo-Sigmoid (SS) Unit; 7—East Bosnian-Durmitor Unit;

8—Dinaric Ophiolite Belt (DOB); 9—Drina-Ivanjica and Pelagonian Units (DIE); 10—Vardar Units (VZ); 11—Lavrion Blueschist Unit; 12—Serbian-Macedonian Massif; 13—Pannonian Basin; 14—Bradanic trough. Ophiolites: a—Ibar; b—Troglov; c—Maljen; d—Zvornik; e—Krivaja-Konjuh; f—Bistrica; g—Zlatibor; h—Pindos; i—North Mirdita (where the study areas are located), l—South Mirdita.

Two ophiolite types are preserved in Albania: MOR-type in the western and SSZ-type in the eastern part of the Mirdita Zone [13,15–17]. The division is based on geological, petrological, geochemical, and mineralogical data [15]. The Western-type ophiolitic series, predominantly lherzolitic, spans a thickness of 2–3 km. Within this sequence, mantle rocks are succeeded by troctolite, gabbro, and pillow basalt. In some cases, the plutonic section is missing, and the basalt directly overlies the ultramafic units [13]. The Eastern-type ophiolitic series is 6–8 km thick. It is composed of dominantly harzburgitic mantle rocks (harzburgite-dunite and dunite with subordinate wehrlite and lherzolite), gabbro, basaltic sheeted dikes, basalt, and boninite [13,15,18]. Both ophiolitic sequences are underlain with metamorphic soles which show similar ages at the western and eastern parts, according to [19–21]. Systematic rejuvenation is detected from south to north (174–168 Ma to 164–160 Ma) indicating a scissor-like closure of the ancient oceanic basin [19]. The ages correlate with the Bajocian–early Bathonian (~168–166 Ma) to late Bathonian–early Callovian (~165–163 Ma) radiolarian cherts overlying the pillow basalts [22,23].

The maximum degree of metamorphism suffered by the Mirdita Zone rocks is of lower greenschist facies, which did not cause significant element mobilization, according to [21].

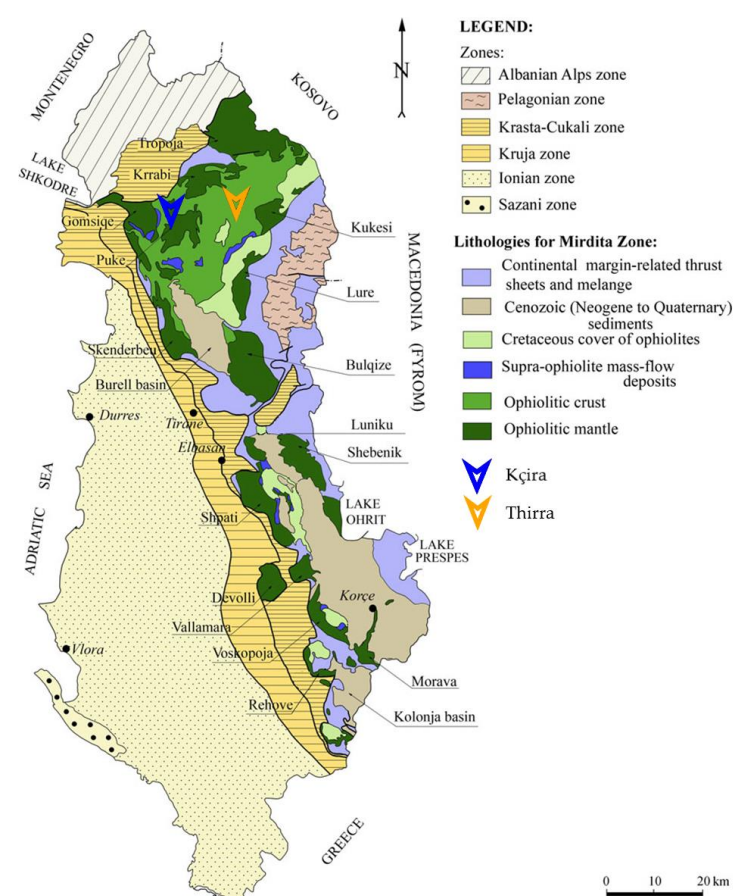


Figure 2. Simplified geological map showing the main tectonic units of Albania, including the Jurassic ophiolites, after [24].

2.1. Ore Deposits of the Kçira Gabbroic Massif

The deposit of Kçira is located in the Kçira Gabbroic Massif, 12 km to the west from Puka town in the western (MOR-type) ophiolite belt (Figures 2 and 3). The most common rock type is gabbro in the area, but gabbro-diabase, gabbronorite, and olivine-gabbro occur as well [4].

According to [25], the primary relationships between the ultrabasic, basic plutonic, and volcanic rocks without significant tectonic overprints are observable in the Western-type ophiolites.

The hydrothermal-metasomatic mineralisation, similarly to other sulphide-bearing quartz veins occurrences in the region, form epigenetic veins in gabbroic rocks, and its mineral composition has most likely a genetic connection with the host, according to [3]. Three mineralisation types are distinguished in this area: in the northern part of the massif, a few 10 m wide copper-chlorite-sulphide type occurs with chalcopyrite, pyrite, and iron-oxides hydroxides; in the southern area, sulphide-bearing quartz type with chalcopyrite, azurite, and iron-hydroxides; and the third type of mineralisation is found in cracks, composed of chalcopyrite, pyrite, and iron-hydroxides in non-altered gabbro [4].

Although the basic macroscopic and mineralogical descriptions of the Kçira Gabbroic Massif are available, the alterations and the geochemical characteristics of the mineralisations are not yet studied.

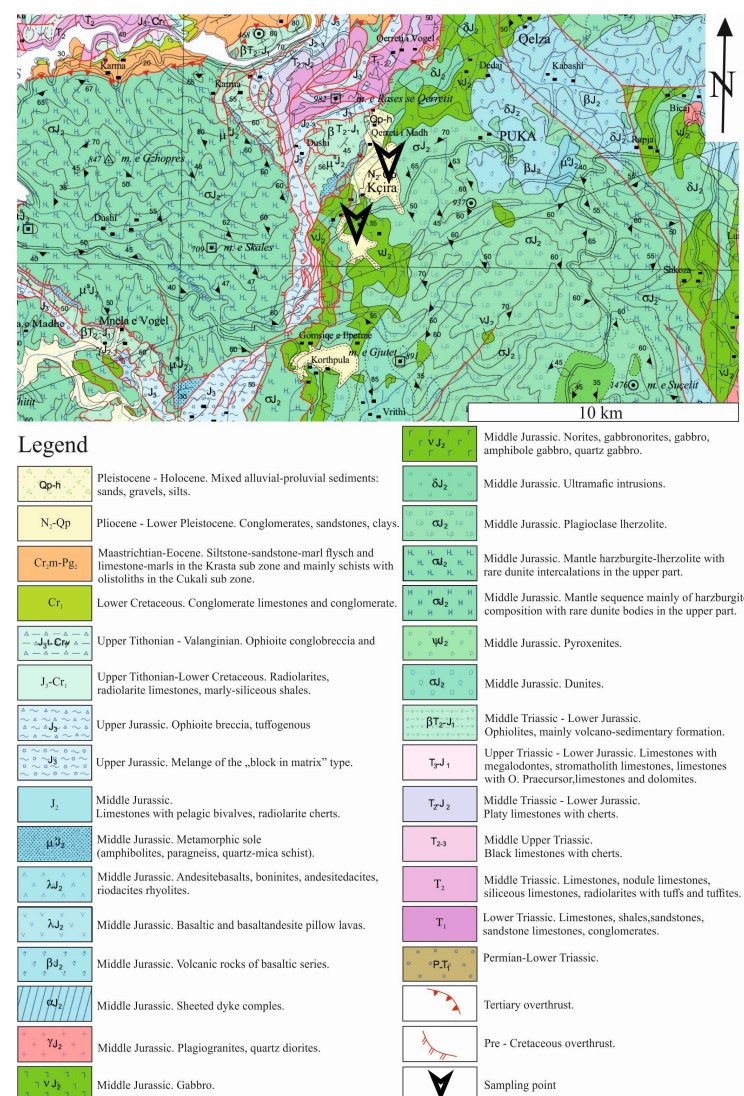


Figure 3. Detailed geological map of the area of the Kçira Gabbroic Massif, after [26].

2.2. Ore Deposits of the Kaptina Gabbroic Massif

Thirra is located in the Kaptina Gabbroic Massif, at the northern part of the eastern (SSZ-type) ophiolite belt (Figure 4). Every part of the ophiolitic series can be observed in this massif, including the plutonic and volcanic units covered by Cretaceous to Cenozoic sediments. The magmatic rocks are andesite, dacite, rhyodacite, and basalt, along with ultrabasic, basic, and neutral plutonic rocks [5]. The most common rock types are gabbro, gabbro-norite, norite, amphibole- and quartz-gabbro, and rarely plagioclase-pyroxenite. The main sulphide mineralisations of the massif are Thirra, Gdeshta, Pista, Shémri, Golaj, and Nikoliq [5]. According to [1], the resources in single orebodies are between 0.5–1 Mt, grading 1%–1.73% Cu, and Au 0.1–0.5 ppm. Ref. [27] suggests that the mineralisations of the Kaptina Massif are formed through moderate temperature hydrothermal metasomatic processes. The ore deposits of the Kaptina Gabbroic Massif are variable, concerning the mineral species and texture; moreover, this variability appears within one deposit as well.

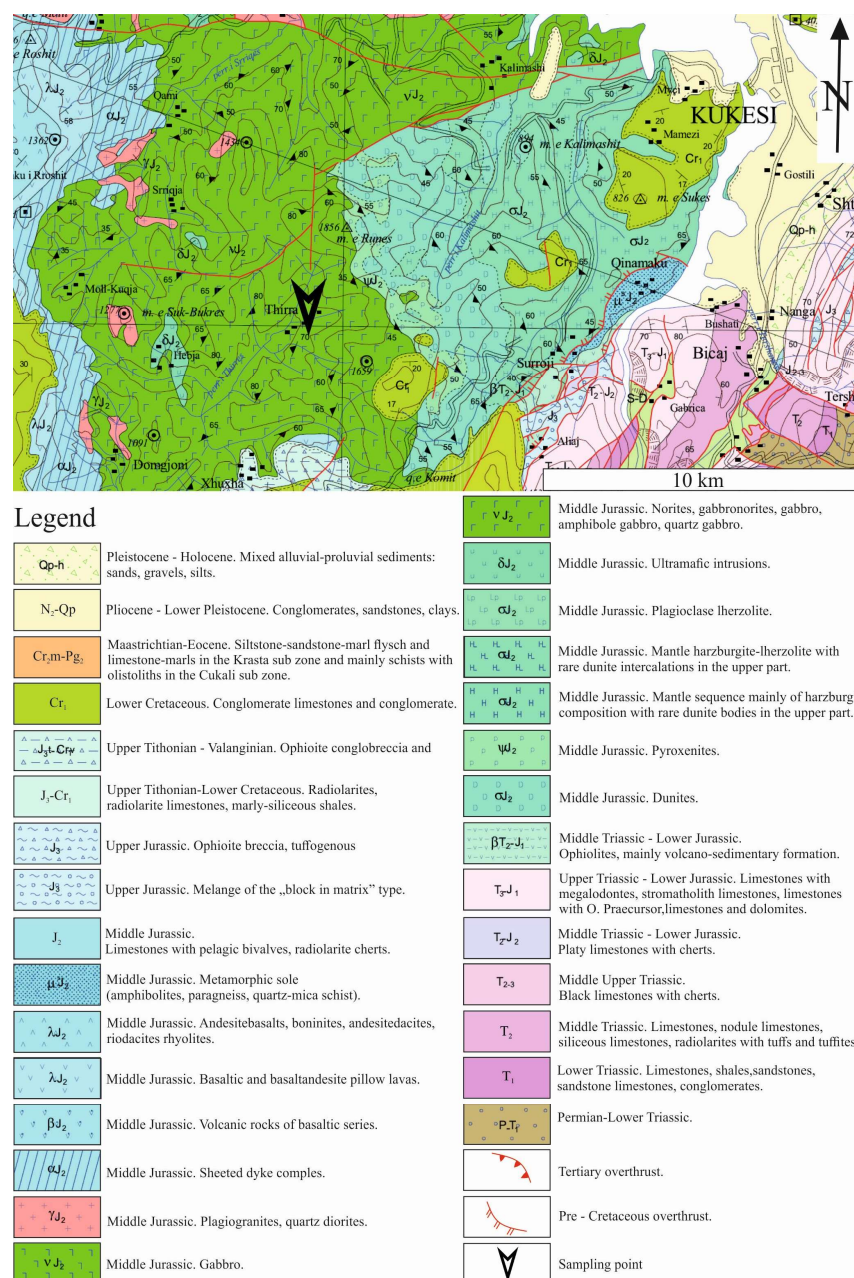


Figure 4. Detailed geological map of the area of the Kaptina Gabbroic Massif, after [26].

The first discovered deposit of the massif is the Thirra deposit, which consists of seven major veins (1, 6, 6b, 6c, 7, 7d, 8/A with 1–3 m width, 100–200 m depth and 200–300 m length) and ten minor ones all with a NE-SW strike [5,27]. Ref. [5] distinguishes six different types of mineralisations here: (1) the most common is the quartz-chalcopyrite type, and besides there are (2) chlorite-chalcopyrite-pyrrhotite, (3) quartz-chalcopyrite-chlorite, (4) chlorite-pyrite-epidote, (5) quartz-chalcopyrite-arsenopyrite, and (6) quartz-chalcopyrite-sphalerite types.

3. Materials and Methods

Field studies were carried out in abandoned mines and natural outcrops of the Kçira Gabbroic Massif and the Kaptina Gabbroic Massif. The aim of the field work was the representative sampling of both relatively fresh and hydrothermally altered host rocks (alteration halo of the mineralisation) as well as the sulphide-bearing quartz veins.

A thin-section petrographic study of host rock samples—with emphasis on the observation of the distinctive textures of magmatic rocks and hydrothermal alteration mineral assemblages—as well as a study of the polished sections of the mineralised veins were performed using polarising microscopes.

The chemical compositions of mineral grains were determined semi-quantitatively using an Amray 1830I scanning electron microscope with an EDAX PV9800 type energy-dispersive X-ray spectroscopy detector (EDS) at the Department of Petrology and Geochemistry, Eötvös Loránd University (Hungary), and they were determined quantitatively using a Jeol Superprobe JXA-8200 type electron microprobe with wavelength-dispersive X-ray spectroscopy (WDS) detector at the Eugen F. Stumpf Laboratory, University of Leoben (Austria). The EDS analyses were completed with focused electron beam with 20 kV accelerating potential, 1 nA beam current, and 100 s detection time. The detection limits were 1.5 wt% for Na₂O, 1 wt% for MgO and Al₂O₃, while they were 0.1 wt% for the other analysed elements. WDS analyses were completed with 15 keV accelerating potential, 10 nA beam current, 1 µm beam diameter, and 20 s (peaks) and 10 s (backgrounds) detection times. The detection limits for the analysed elements are as follows: As 300 ppm; S 150 ppm; Bi 400 ppm; Zn 200 ppm; Fe 150 ppm; Se 300 ppm; Te 150 ppm; Ni 100 ppm; Cu 500 ppm; Ag 300 ppm; Pb 400 ppm; Sb 600 ppm; Co 200 ppm; Au 500 ppm; Tl 500 ppm. Both instruments were calibrated using well-known natural and synthetic standards.

X-ray Powder Diffraction (XRPD, at the Department of Mineralogy of the Eötvös Loránd University) was used for the determination of fine-grained mineral phases. A Siemens D-5000 type diffractometer with Bragg-Brentano geometric emission (Θ - Θ working method, Cu K α , $\lambda = 0.154178$ nm), a secondary graphite crystal monochromator, and a scintillation detector were used together with the EVA software (version 16.0.0.0; Bruker-AXS Diffrac Plus) for data analysis.

Preliminary whole-rock geochemical analyses, inductively coupled plasma—optical emission spectrometry (ICP OES) were carried out at the Laboratory of the Supervisory Authority of Regulatory Affairs (SARA) (former Mining and Geological Survey of Hungary). Analytical procedures are described in the accreditation documentation of the laboratory (MSZ 21470-50:2006 and MÁFI 11.12:2012). The detection limits for major elements are SiO₂ 0.5 wt%, Al₂O₃ 0.5 wt%, Fe 0.5 wt%, MnO 0.01 wt%, BaO 0.01 wt%, S 0.01 wt%, SrO 0.01 wt%, while for trace elements As 50 ppm, Co 50 ppm, Cr 25 ppm, Cu 25 ppm, Ni 25 ppm, Pb 50 ppm, V 25 ppm, Zn 25 ppm, Ag 10 ppm, Au 2.5 ppm.

4. Results

4.1. Field Study

The sampling points of the mineralisation of the Kçira Gabbroic Massif are in Kçira, in the so-called Puka area: an abandoned mine, at the coordinates of 42°00'09.8" N, 19°49'08.8" E and a natural outcrop, with coordinates 42°00'26.8" N, 19°48'56.5" E (Figure 5). The latter is a 10–20 cm wide sulphide-bearing quartz vein in a dry stream with a strongly altered surface. The gangue minerals are 5%–10% quartz with the same amount of chlorite,

while the sulphides (80%–90%) are massive chalcopyrite with 0.5 mm disseminated pyrite crystals. The host rock is a moderately altered gabbroic rock with a limonitic surface. The former area is an abandoned underground Cu-mine that operated in the second half of the 20th century, related to the same mineralisation system. Since the galleries are not in a good condition nowadays, the samples were collected from the surface (outcropping host rocks and waste dump).

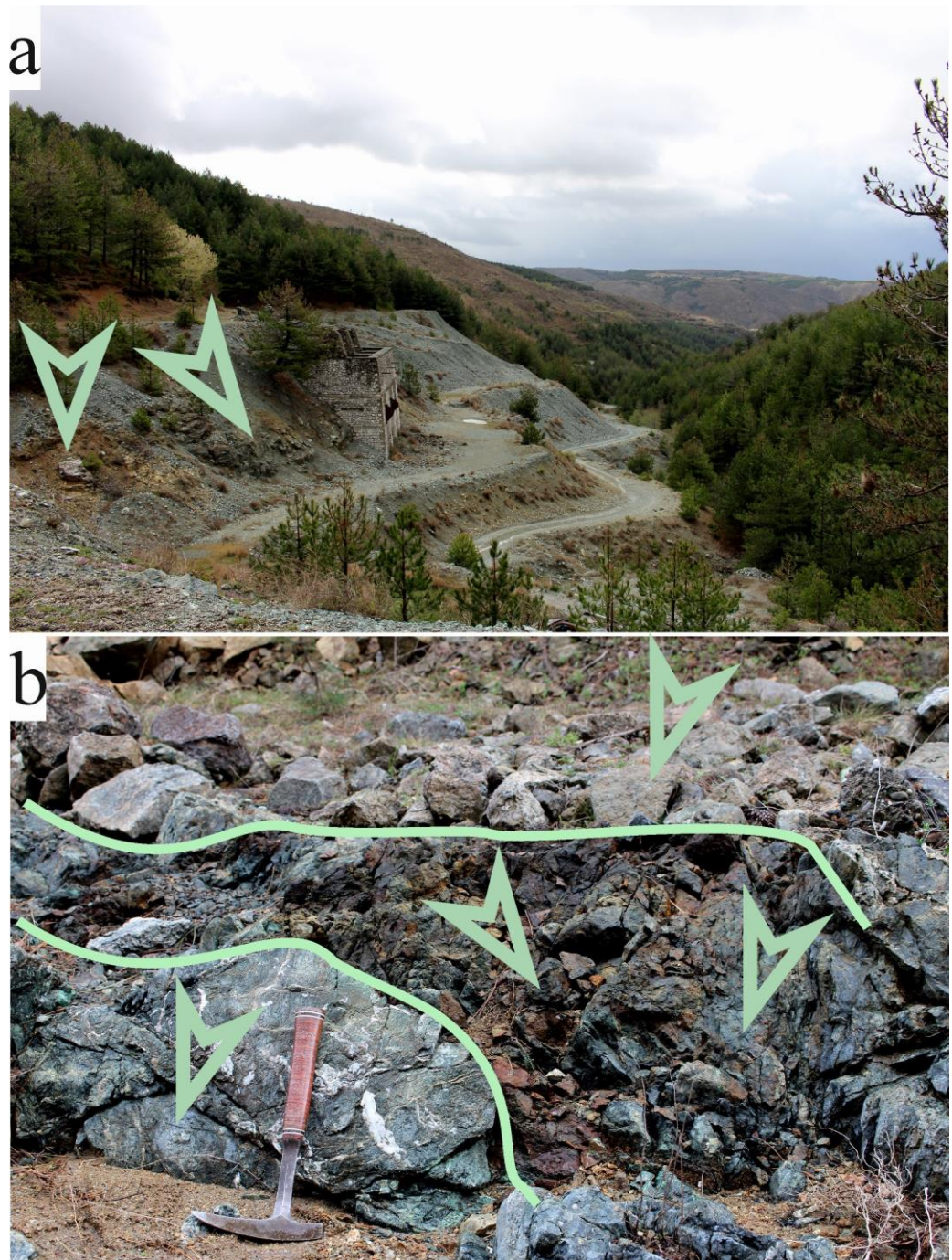


Figure 5. Photos of sampling points of Kçira. (a) Abandoned Cu-mine with outcropping rocks and waste. (b) Sulphide-rich vein in altered gabbroic host rock. Arrows indicate the sampling points.

The sampling area in the Kaptina Gabbroic Massif is Thirra, an abandoned mine from the 20th century. The samples are collected from the 6c vein, $42^{\circ}00'03.1''$ N, $20^{\circ}12'11.0''$ E (Figure 6). The outcropping part of the vein is 1 m wide and 1.5 m long. It represents

the quartz-chalcopyrite-arsenopyrite type of the six mineralisation types identified by [5]. Massive chalcopyrite, pyrrhotite, and 0.2–0.5 mm pyrite occur in the vein with the same amount of gangue minerals, quartz and chlorite. Close to the mineralisation, the host is a strongly altered (chloritised and argillitised) gabbroic rock, while it is only slightly altered ~30 cm further.

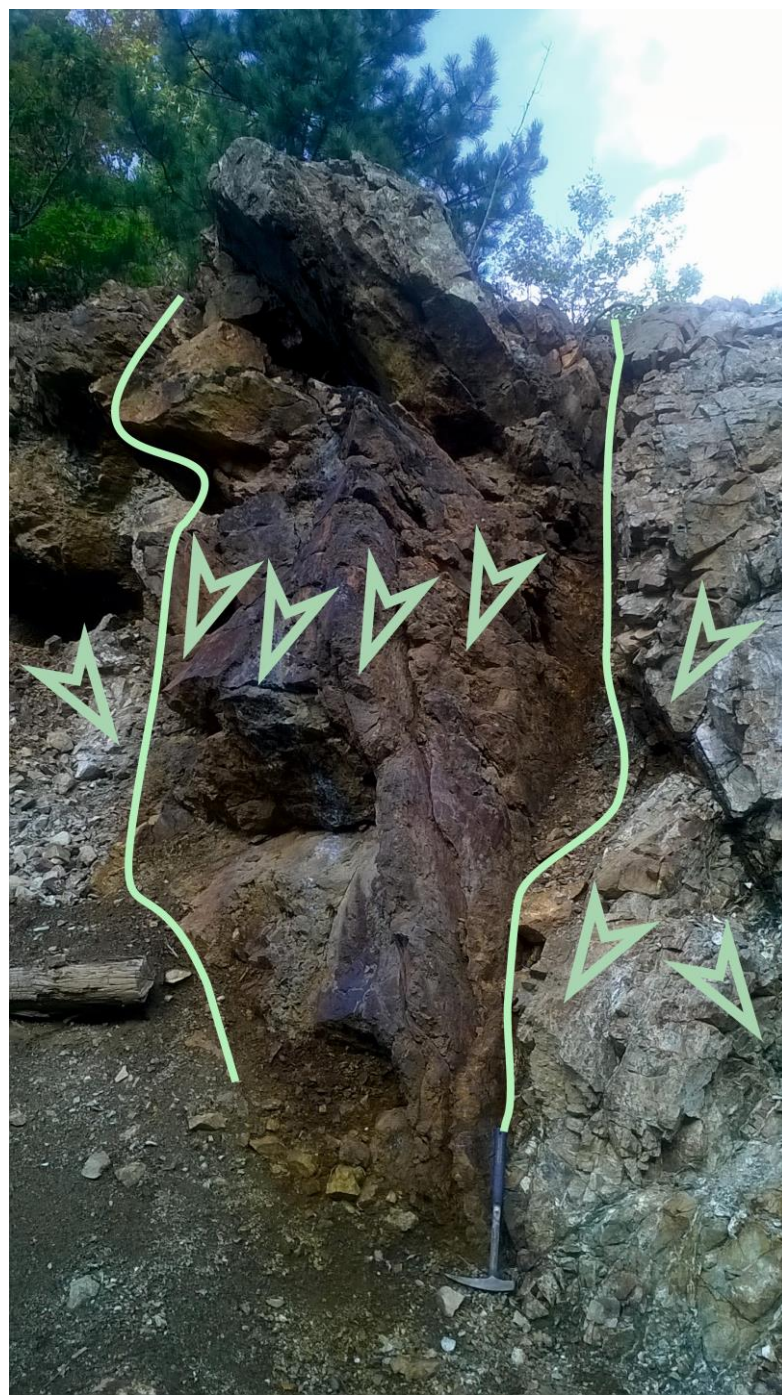


Figure 6. Outcropping mineralised vein in the abandoned Cu-mine of Thirra with the sampling points indicated.

4.2. Host Rock Petrography and Mineral Chemistry

Differently altered mafic plutonic rocks were found in the study areas. Based on macroscopic observation, these are medium-grained, holocrystalline gabbroic rocks with chloritised mafic crystals and 0.1–2.0 mm wide white and grey veinlets.

At Kçira, the modal composition shows that the host rocks are gabbro and gabbronorite, composed of xenomorphic and hypidiomorphic plagioclase (50%–70%) and pyroxene (10%–30%) crystals with panallotriomorphic, subophitic, and ophitic texture, crosscut with veinlets (10%) (Figure 7b,d,f).

The size of the xenomorphic and hypidiomorphic plagioclase crystals is mainly between 1 and 3 mm. According to the SEM-EDS analyses, the unaltered crystals are anorthite (An_{91-97}) and bytownite (An_{75-85}), while plagioclases in the altered parts are enriched in Na_2O (between An_{59} and An_{12}) (Figure 7g). Additionally, 100 μm sized clinopyroxene and 10–100 μm sized chalcopyrite, pyrite, and rarely apatite inclusions occur in the plagioclase crystals (Figure 7d). Sericite is the most common alteration mineral, while in rare cases the cores of the plagioclase are calcitised.

The mafic phase is clinopyroxene with 0.1–1 mm sized xenomorphic grains. These are Ca-Mg-Fe, quad pyroxenes, within the range of augite (based on the nomenclature of [28]). However, two distinct chemical compositions occur: Ca-rich and Ca-poor augite ($Mg_{0.87}Ca_{0.82}Fe_{0.22}Al_{0.12}Si_{1.96}O_6$ and $Mg_{0.94}Ca_{0.47}Fe_{0.32}Al_{0.21}Si_{1.98}O_6$); the latter composition also appears as rims on the Ca-rich augite grains (Figure 7h). Furthermore, 100–500 μm sized plagioclase grains and a few 10 μm sized chalcopyrite are enclosed in the clinopyroxene crystals. Additionally, chloritisation can be observed at the rims and fissures of the grains.

Rarely, chlorite pseudomorphs after orthopyroxene can be found with remnants of orthopyroxene in the core. If present, the orthopyroxene gives 10%–15% of the rock, and 40% among the total pyroxenes.

Primary ilmenite grains of 0.5–1.0 mm size occur rarely (<5%) interstitially among the plagioclase laths.

The nature of the alteration is the same throughout the host rocks, but the intensity changes with the distance from the mineralised veins. Besides the above mentioned chloritisation, sericitisation and calcitisation of the main rock-forming minerals, there are 10–100 μm thin veinlets filled with ~5–50 μm sized xenomorphic, mostly Fe-poor epidote (Table 1), prehnite, chlorite, calcite, quartz, and albite (An_5) (Figure 7a–c,e). Additionally, 100 μm sized xenomorphic titanite was detectable accompanying the epidote veins (Figure 7e,f).

Table 1. SEM-EDS analyses of selected epidote grains from the altered host rocks and mineralised veins. n = number of analyses; * total iron expressed as Fe_2O_3 (recalculated by the software of the EDAX PV9800 EDS detector); cation values are given in apfu. # $Fe = Fe^{3+}/(Fe^{3+} + Al^{3+})$.

Locality	Rock Type	n	SiO_2	Al_2O_3	Fe_2O_3 *	CaO	Total	Si	Al	Fe	Ca	Total	Fe #
Puka	altered host	5	39.49 ± 0.61	26.75 ± 0.60	7.98 ± 0.77	23.78 ± 0.24	98	6.14 ± 0.08	4.90 ± 0.10	0.93 ± 0.09	3.96 ± 0.05	15.94 ± 0.04	0.16 ± 0.02
	altered host	17	38.40 ± 0.58	25.38 ± 1.32	10.51 ± 1.92	23.70 ± 0.56	98	6.04 ± 0.06	4.70 ± 0.21	1.25 ± 0.23	3.99 ± 0.10	15.99 ± 0.05	0.21 ± 0.04
	mineralised vein	4	39.32 ± 0.16	24.20 ± 1.30	10.48 ± 1.46	24.00 ± 0.25	98	6.19 ± 0.04	4.48 ± 0.22	1.24 ± 0.18	3.99 ± 0.03	15.94 ± 0.02	0.22 ± 0.03
Thirra	altered host	5	39.05 ± 1.12	24.62 ± 1.06	10.52 ± 1.35	23.81 ± 1.20	98	6.14 ± 0.13	4.56 ± 0.18	1.24 ± 0.16	4.01 ± 0.22	15.96 ± 0.03	0.21 ± 0.03

In Thirra, the host rocks are gabbro and gabbronorite with panallotriomorphic granular and hypidiomorphic granular textures (Figure 8a,b). The rock-forming minerals are mainly xenomorphic plagioclase (55%–65%) and clinopyroxene (30%–40%), though in some cases orthopyroxene also occurs (~20%).

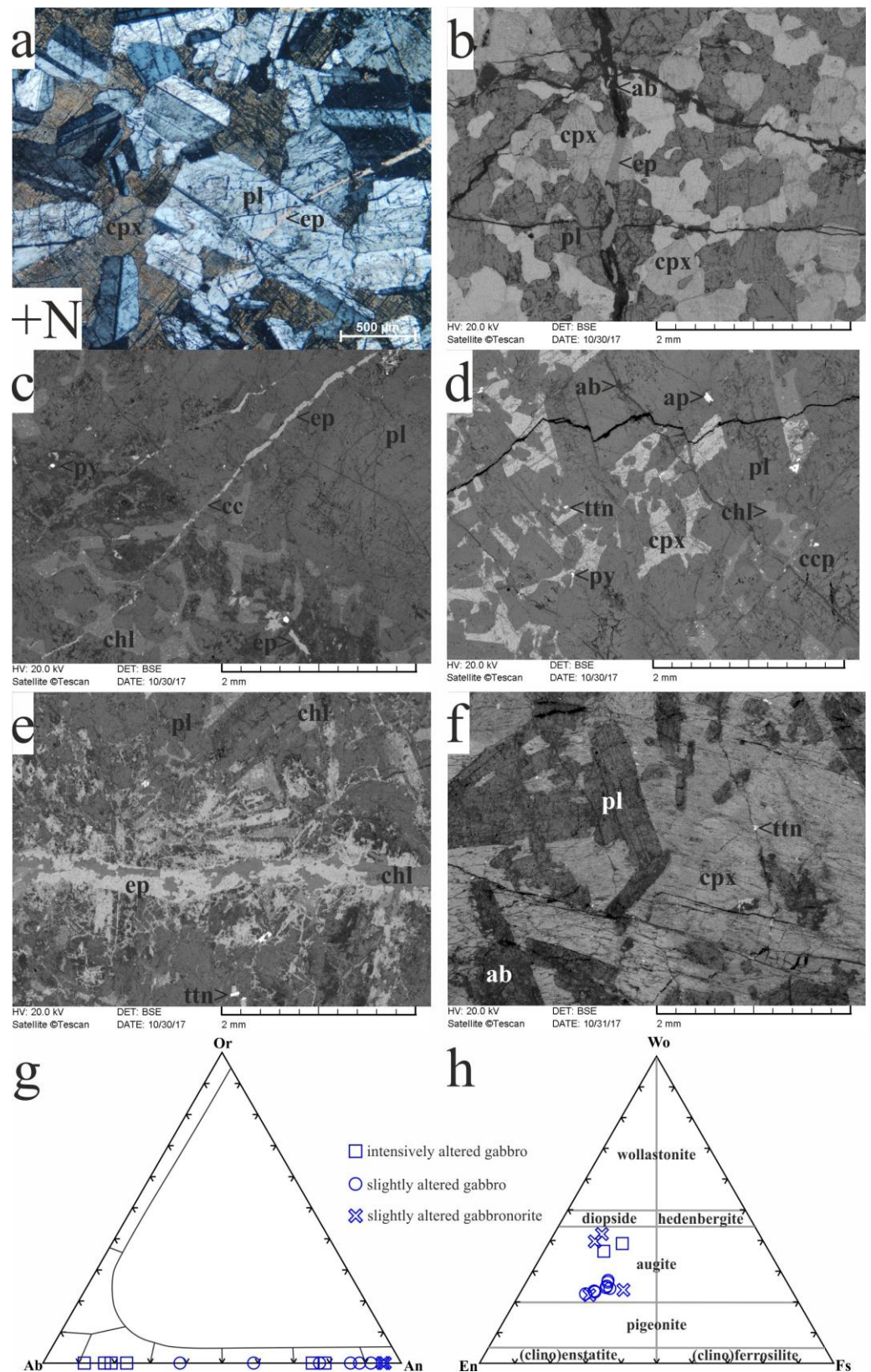


Figure 7. (a–f) Microphotograph and BSE images of host rock samples from Kçira. (g) Ternary diagram of the analysed plagioclase grains, based on [29]. (h) Ternary diagram of the analysed pyroxene grains, based on [28]. cpx = clinopyroxene, pl = plagioclase, ab = albite, chl = chlorite, ep = epidote, cc = calcite, ap = apatite, ttn = titanite, py = pyrite, ccp = chalcopyrite.

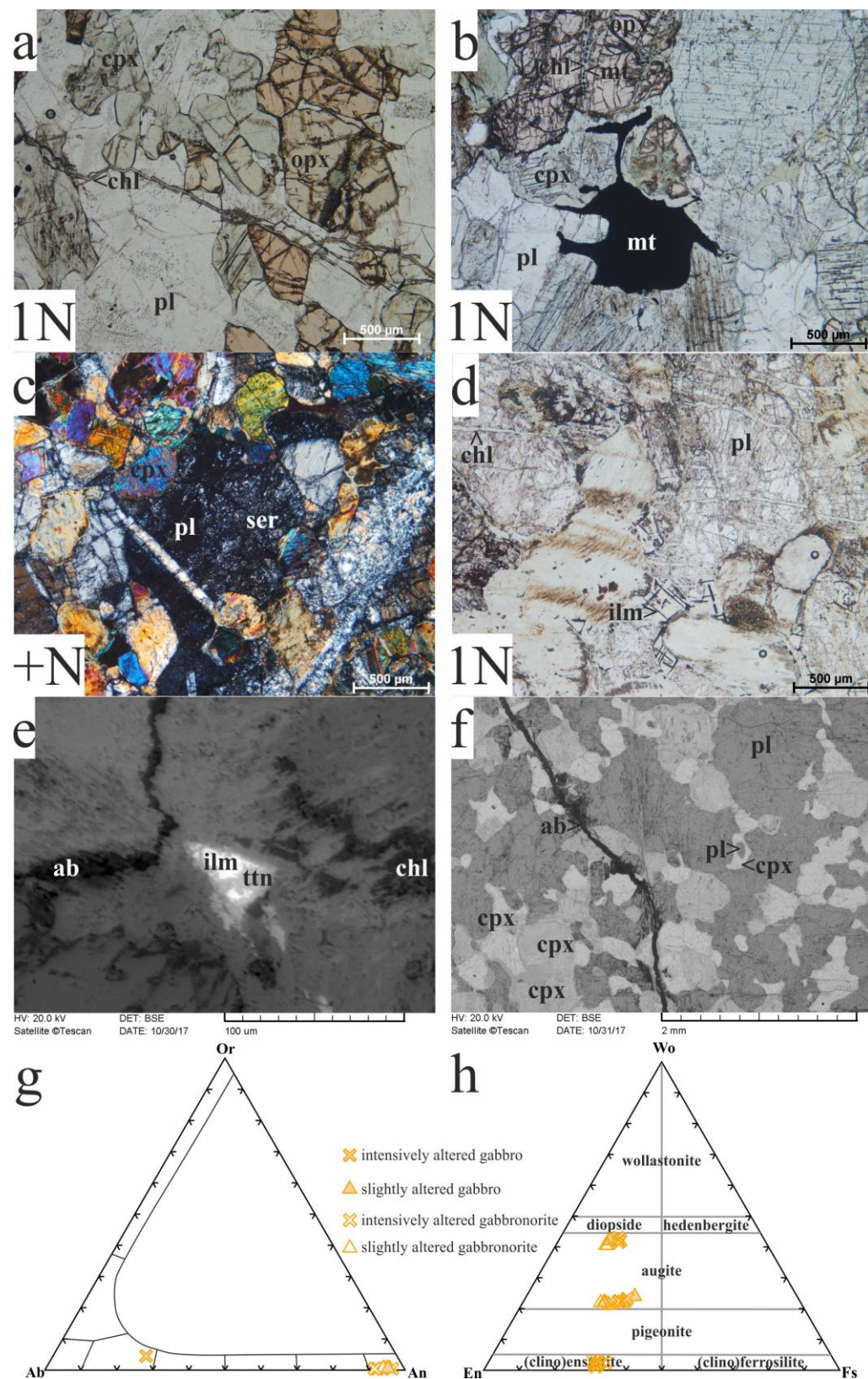


Figure 8. (a–f), Microphotographs and BSE images of host rock samples from Thirra. (g) Ternary diagram of the analysed plagioclase grains, based on [29]. (h) Ternary diagram of the analysed pyroxene grains, based on [28]. cpx = clinopyroxene, opx = orthopyroxene, pl = plagioclase, mt = magnetite, chl = chlorite, ser = sericite, ilm = ilmenite, tttn = titanite, ab = albite.

The size of the plagioclase crystals is mostly between 0.5 and 1.5 mm except for the coarser grained samples, where 2.0–5.0 mm sized crystals occur. They are usually xenomorphic, and are rarely hypidiomorphic anorthite (An_{92-97}) crystals, with apparent polysynthetic twinning (Figure 8c,g). The crystals often enclose clinopyroxene and primary hypidiomorphic and xenomorphic magnetite grains (0.01–0.1 mm size). In some cases, the plagioclase crystals have a spongy core, and melt inclusions mark the growth zonation in some grains. Sericitisation can be observed in the core of this mineral (Figure 8c).

The clinopyroxene grains are usually 0.2–1.5 mm in size or 2.0–5.0 mm in the case of coarse grained rocks with xenomorphic or hypidiomorphic crystal shape. Anorthite can be observed occasionally as inclusions of clinopyroxenes. The occurring clinopyroxene crystals are Ca-Mg-Fe, quad pyroxenes, within the range of augite, based on the nomenclature of [28]. Based on the mineral chemical analysis, two populations of clinopyroxene can be distinguished: Ca-rich and Ca-poor, both of them within the field of augite ($Mg_{0.88}Ca_{0.79}Fe_{0.23}Al_{0.15}Si_{1.95}O_6$ and $Mg_{1.1}Ca_{0.44}Fe_{0.22}Al_{0.17}Si_{1.99}O_6$). The Ca-poor augites are often enclosed in Ca-rich ones, while sometimes the former one surrounds the Ca-rich augites (Figure 8f,h).

Chloritisation is a common phenomenon of the clinopyroxene grains. In extreme cases, ilmenite lamellae appear in chlorite mass, marking the former presence of clinopyroxene, which suffered intense alteration (Figure 8a,b,d).

In two samples, orthopyroxene (hypersthene) occurs in around 20% (1–3 mm in size). It usually contains 50 μm sized clinopyroxene inclusions. Due to intense alteration (uralitisation and opacitisation), actinolite/tremolite and chlorite with magnetite occur in the rims and fissures of the orthopyroxene grains (Figure 8a,b).

Magnetite is a common accessory mineral in gabbroic rocks; xenomorphic inclusions (0.05–0.1 mm in size) in orthopyroxene and plagioclase are common; and interstitial grains occur as well (Figure 8b). Ilmenite accompanies magnetite occasionally, while xenomorphic chalcopyrite and pyrite grains also appear in plagioclase laths.

The alteration is similar to the samples of Kçira: chloritisation of the mafic, sericitisation of the felsic rock-forming minerals. Magnetite, quartz, oligoclase (An_{28}), and titanite after ilmenite also occur as alteration products (Figure 8e).

The cross-cutting veins are filled with epidote (Table 1), chlorite, and sodic plagioclase (An_{11}) (Figure 8e,f).

XRPD analyses on the intensely altered host rock samples representing the alteration halo of the ore mineralisation revealed the presence of chlorite, actinolite/tremolite, prehnite, epidote, smectite/vermiculite, and laumontite in Thirra, while chlorite, actinolite/tremolite, plagioclase, prehnite, calcite, and laumontite are present in Kçira.

4.3. Ore Mineralisation Petrography and Mineral Chemistry

The ore mineralisation of Kçira is mainly composed of massive chalcopyrite (60%) and disseminated idiomorphic, sometimes hypidiomorphic pyrite with a resorbed rim (5%) (Figure 9a,b). 5–10 μm xenomorphic AgAu-, Ni-telluride, native tellurium (newly described species from the area), and CoNi-sulphide grains were also detected in less than 1% (Figure 9d,e). AgAu-telluride and native tellurium grains occur along fissures—associated with chalcopyrite—in pyrite, and the latter as inclusions in chalcopyrite. Ni-telluride also appears as inclusions in chalcopyrite. The gangue minerals are xenomorphic quartz (~1 mm in size) (15%) and chlorite (15%), idiomorphic 100–200 μm long prehnite and epidote laths (10%), and 10–20 μm xenomorphic titanite (<1%) grains, which are disseminated in the massive chalcopyrite and in the chlorite (Figure 9c,d,f; Table 1).

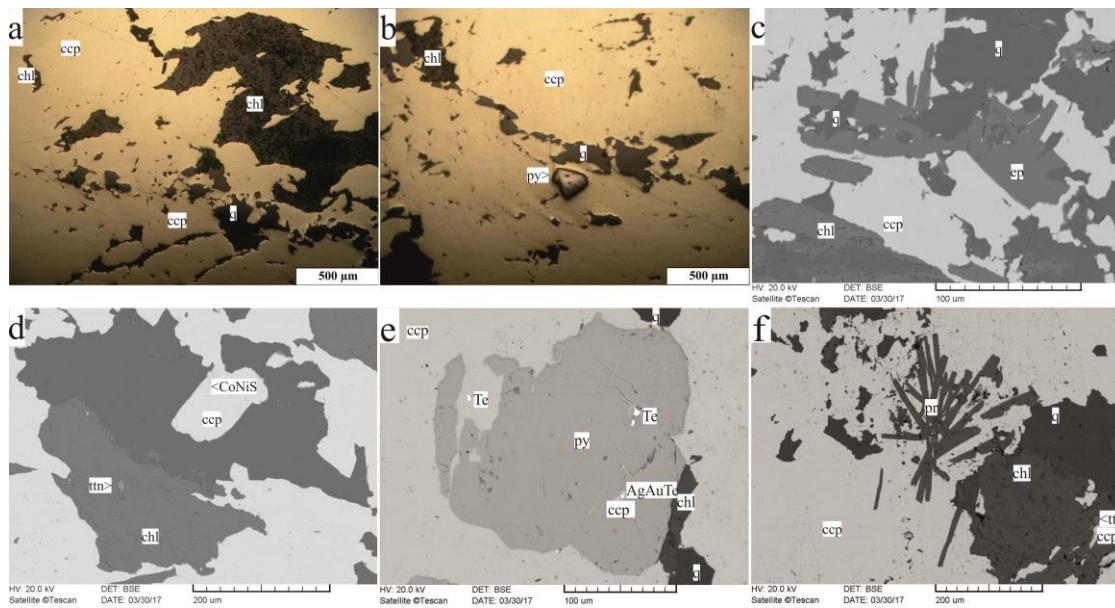


Figure 9. Reflected light microphotographs (a,b) and BSE images (c–f) of the ore samples from Kçira. ccp = chalcopyrite, chl = chlorite, py = pyrite, q = quartz, ep = epidote, ttn = titanite, pr = prehnite.

The ore mineralisation occurs with stockwork texture in Thirra, where two types can be distinguished based on the occurring minerals: pyrrhotite-chalcopyrite and chalcopyrite-arsenopyrite-pyrite types. The former is composed mostly of xenomorphic chalcopyrite and pyrrhotite in 30%–30%, alongside those disseminated, 0.5 mm idiomorphic-hypidiomorphic pyrite (5%) and 50–500 µm xenomorphic sphalerite grains occur in the samples (Figure 10a,b). Quartz (30%, 0.5–1.0 cm in size) and chlorite (<5%) are the gangue phases. Quartz grains are often crosscut with Fe-oxide/hydroxide, “limonitic”, and pyrite veins, while chlorite occurs in chalcopyrite or quartz, and sometimes it crosscuts the samples, as the last phase of the hydrothermal process (Figure 10e). Additionally, ilvaite, a newly described mineral of this locality was detected using SEM-EDS. Ilvaite occurs in veins with chalcopyrite and either as inclusions in chalcopyrite or as the host of it (Figure 10f).

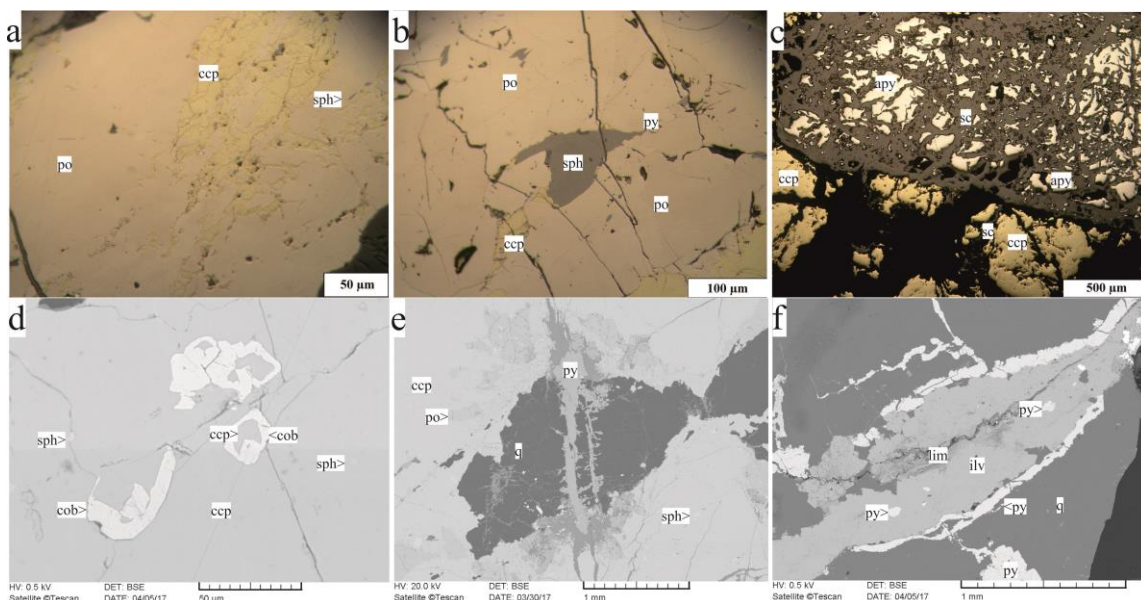


Figure 10. Reflected light microphotographs (a–c) and BSE images (d–f) of the ore samples from Thirra. ccp = chalcopyrite, po = pyrrhotite, py = pyrite, sph = sphalerite, apy = arsenopyrite, sc = scorodite, cob = cobaltite, q = quartz, lim = limonite, ilv = ilvaite.

In some cases, chalcopyrite occurs as inclusions in quartz (0.1 mm in size), while the massive chalcopyrite encloses quartz, chlorite, sphalerite, pyrite, and pyrrhotite grains. The massive pyrrhotite contains sphalerite, pyrite, and quartz inclusions. The pyrite grains frequently have altered rims with Fe-oxides/hydroxides, and there are some veins in quartz, filled with the altered pyrite. There are sphalerite inclusions—often with chalcopyrite disease—in pyrite, chalcopyrite, and pyrrhotite (Figure 10b). Furthermore, 5–20 µm xenomorphic and idiomorphic cobaltite grains occur in chalcopyrite and also in quartz, and cobaltite encloses chalcopyrite occasionally (Figure 10d).

The chalcopyrite-arsenopyrite-pyrite type is a hydrothermal breccia, where sulphides with alteration phases make up the matrix (40%) between the quartz clasts (60%). The matrix is composed of chalcopyrite (30%), arsenopyrite (20%), and pyrite (5%–10%) (Figure 10c). Based on microscopic and SEM-EDS analyses, the 0.5–1 mm fragmented arsenopyrite grains are strongly altered to scorodite (they are also newly described from the area), which makes up 40% of the matrix. The xenomorphic chalcopyrite grains are also fragmented where scorodite is the matrix. Quartz is found as inclusion in chalcopyrite, and it encloses 0.1 mm chalcopyrite grains as well. Chalcopyrite veins even crosscut the arsenopyrite mass. Additionally, 0.2 mm hypidiomorphic and idiomorphic pyrite grains occur as inclusions of quartz and in the matrix as well. In some cases, square-shaped arsenopyrite grains are identified which can be pseudomorphs after pyrite. In less than 5%, 50 µm sphalerite grains occur in chalcopyrite.

4.4. EPMA Analyses of Pyrite

The iron contents of the analysed pyrite grains are between 46.02 and 47.78 wt% in Thirra and 45.51–47.70 wt% in Kçira, while the sulphur contents vary between 52.30 and 53.64 wt% in Thirra and 52.23 and 53.32 wt% in Kçira. These indicate different quantities and quality of trace element content [30]. Pb- and Ag-contents are higher in Thirra, while Ni- and Cu-contents are higher in Kçira, the concentrations of Bi and Tl are mostly under the detection limit in all cases (Table 2).

Table 2. Results of EPMA analyses of pyrite grains (Fe and S contents are given in wt%, other elements in ppm, d.l. = detection limit, - = below detection limit).

	Fe	S	Cu	Zn	Pb	Bi	As	Se	Co	Ni	Te	Ag	Au	Tl	Total
	d.l. (ppm)	150	150	500	200	400	400	300	300	200	100	150	300	500	500
Thirra	47.27	53.14	-	320	-	-	-	-	1040	-	-	-	-	-	100.61
	47.51	53.29	-	-	-	-	-	-	1060	-	-	-	680	-	101.03
	47.27	53.15	-	-	-	-	-	-	830	-	-	320	-	-	100.60
	47.57	53.36	-	-	-	-	-	-	1410	-	-	-	-	-	101.11
	47.66	52.80	-	-	-	-	-	310	460	-	-	-	-	-	100.58
	47.78	53.35	830	-	770	-	-	-	-	-	-	-	-	-	101.34
	47.36	52.69	-	-	-	-	-	300	1410	-	-	-	-	-	100.21
	47.39	53.20	-	-	-	-	-	-	1320	-	-	-	-	-	100.81
	46.48	53.23	720	-	-	-	-	1270	1090	-	-	340	-	-	100.10
	47.39	52.68	950	-	-	-	-	-	640	-	-	300	-	1000	100.36
	46.79	52.73	-	230	-	-	-	-	900	-	-	800	-	-	99.75
	46.91	52.65	-	-	-	-	-	-	2990	-	200	-	-	-	99.89
	47.31	52.40	-	-	-	460	800	440	890	-	230	-	1170	-	100.13
	46.99	52.39	1380	-	-	-	380	600	880	-	150	-	-	-	99.76
	46.94	52.61	1040	-	-	-	-	-	1440	-	-	-	-	-	99.82
	46.30	53.04	2930	-	-	-	470	740	2600	-	-	-	1510	-	100.17
	47.28	52.36	-	-	-	-	-	-	1570	-	-	-	-	-	99.87
	46.54	53.27	-	-	-	-	-	-	1180	-	250	-	-	-	99.97
	47.24	52.80	-	-	-	-	-	2500	2300	-	-	-	-	-	100.55
	47.50	52.74	-	-	-	-	-	470	1240	-	190	-	-	-	100.45
	47.64	53.01	-	-	-	-	-	-	300	-	-	-	-	-	100.71
	46.93	53.43	-	-	-	-	-	1100	520	-	-	-	-	-	100.53
	47.02	52.75	-	-	770	-	1000	700	1310	-	-	490	-	-	100.20
	47.02	53.40	780	-	-	-	710	-	850	-	-	-	-	-	100.71

Table 2. Cont.

	Fe	S	Cu	Zn	Pb	Bi	As	Se	Co	Ni	Te	Ag	Au	Tl	Total
d.l. (ppm)	150	150	500	200	400	400	300	300	200	100	150	300	500	500	
	46.92	53.01	-	-	-	-	-	-	1190	-	-	-	780	-	100.21
	47.33	53.14	620	-	-	-	610	-	820	-	-	-	530	-	100.75
	46.81	52.54	1480	-	-	-	-	-	1560	-	-	-	-	-	99.66
	46.41	52.81	-	-	-	-	520	-	1280	-	-	-	-	-	99.45
	46.25	52.73	4660	-	-	-	-	710	910	-	-	-	-	-	99.61
	46.19	52.92	5360	-	-	-	-	510	520	-	190	-	-	-	99.82
	46.14	52.30	6050	-	-	-	-	-	680	-	-	-	-	-	99.14
	47.08	52.84	-	-	-	-	400	-	500	-	-	-	-	-	100.01
	47.03	52.95	-	-	-	-	-	740	880	-	390	-	-	-	100.25
	46.35	52.77	2430	-	-	-	-	-	1530	-	-	-	-	-	99.53
	46.83	52.87	-	-	490	-	-	-	540	-	-	-	-	-	99.80
	46.49	53.05	1300	-	-	-	670	950	770	-	260	760	-	-	100.04
	46.32	52.98	540	-	410	-	-	1110	720	-	-	-	-	-	99.60
	46.60	52.85	1080	-	-	-	-	1060	610	-	-	-	-	-	99.76
	46.87	52.87	1980	-	-	-	-	-	1330	100	-	-	-	-	100.15
	46.85	52.86	510	-	-	-	-	-	1120	-	-	-	-	-	99.93
	47.61	53.06	-	-	-	-	-	560	450	-	-	-	-	-	100.87
	46.94	52.98	-	-	-	-	430	430	760	120	-	-	-	-	100.11
	46.32	53.64	-	-	-	-	380	-	410	-	170	340	-	-	100.09
	46.25	52.70	-	-	-	-	1140	-	570	-	-	-	-	-	99.17
	46.07	52.90	-	-	-	-	400	-	-	-	-	-	730	-	99.14
	46.61	53.55	1190	-	-	-	-	-	1470	-	-	400	-	-	100.50
	47.52	52.75	4800	250	-	-	-	-	2340	-	-	-	-	-	101.05
	46.72	52.57	2550	-	-	-	-	-	1190	100	-	-	-	-	99.69
	46.27	53.59	-	-	-	-	-	-	950	-	-	-	-	-	99.97
	46.41	53.53	-	-	-	-	310	-	600	-	-	670	-	-	100.13
	46.34	53.02	-	-	620	-	500	-	520	-	-	770	-	-	99.63
Thirra	46.72	53.48	530	-	-	-	440	820	-	-	-	-	-	-	100.41
	46.78	52.69	510	-	-	-	440	970	820	-	-	920	-	-	99.85
	47.05	52.47	510	-	870	-	-	2420	2510	-	-	720	-	-	100.25
	46.99	53.08	570	-	700	-	-	-	1440	-	-	580	-	-	100.41
	46.87	52.47	-	-	-	-	2860	2140	-	390	350	-	-	-	99.97
	46.22	52.99	-	-	-	-	-	-	1670	-	-	-	-	-	99.40
	46.83	52.79	-	-	1190	-	1010	2290	2570	210	-	-	-	-	100.38
	46.48	52.97	-	-	-	-	300	2050	1830	130	-	-	-	-	99.88
	46.51	52.91	-	-	-	-	1110	2030	2780	110	230	-	770	-	100.13
	46.69	52.40	-	-	-	-	510	1720	1230	-	-	-	-	-	99.46
	46.84	52.95	550	-	-	-	-	-	840	-	-	-	-	-	99.93
	46.45	52.76	-	-	-	-	370	1790	-	-	-	-	-	-	99.44
	46.61	52.70	1100	-	490	-	-	1510	1980	200	-	310	-	-	99.88
	46.08	52.99	-	-	-	480	-	680	1570	290	-	670	-	-	99.49
	46.73	53.36	1540	-	-	-	300	3450	1640	140	-	-	-	-	100.85
	46.02	52.81	-	-	-	490	-	1830	-	-	-	-	-	-	99.08
	47.10	52.92	-	-	-	340	790	990	-	-	-	-	-	-	100.29
	46.28	52.91	930	-	590	-	-	1390	1310	-	-	370	720	-	99.73
	46.70	52.64	2390	-	-	-	440	1220	-	230	-	720	-	-	99.87
	46.63	52.90	3270	-	-	-	1500	670	140	-	370	-	-	-	100.13
	46.84	53.17	3170	-	480	-	680	740	1120	-	-	400	-	-	100.67
	46.81	52.60	-	-	-	-	970	1570	-	-	-	-	-	-	99.72
	46.83	52.53	-	-	-	-	1770	2090	-	-	-	-	-	-	99.81
	46.75	52.86	-	-	-	-	320	1850	-	-	-	860	810	-	100.04
	46.44	52.92	-	-	-	-	750	1820	-	200	-	-	-	-	99.69
	46.71	52.62	-	-	-	310	-	1950	-	-	-	-	-	-	99.56
	46.19	52.99	-	-	-	620	1920	2470	-	-	-	-	-	-	99.69
	46.25	52.93	-	-	-	-	660	1780	-	-	-	-	-	-	99.44
	46.56	52.71	-	-	-	700	1990	1560	-	-	450	-	-	-	99.73
Kcira	46.71	53.32	-	-	-	-	-	5920	1400	490	-	-	-	-	100.87
	46.36	53.20	-	-	-	-	680	-	4730	1100	-	-	-	-	100.22
	46.70	53.10	-	-	-	-	-	600	5310	640	-	-	-	-	100.48
	45.86	52.46	-	-	1180	-	-	960	5920	780	-	-	-	-	99.22
	46.97	52.92	-	-	590	-	-	-	3140	800	180	-	-	-	100.37
	46.38	52.72	1050	-	-	-	-	410	2660	720	270	-	520	-	99.67
	46.34	52.93	3060	-	-	-	-	570	3530	640	-	-	-	-	100.05
	46.08	52.92	4700	-	-	-	-	740	3140	1220	-	-	-	-	99.99
	47.40	52.98	810	-	-	-	1280	300	730	-	550	-	-	-	100.80

Table 2. Cont.

	Fe	S	Cu	Zn	Pb	Bi	As	Se	Co	Ni	Te	Ag	Au	Tl	Total
d.l. (ppm)	150	150	500	200	400	400	300	300	200	100	150	300	500	500	
Kçira	46.31	53.12	1190	-	-	-	-	-	570	-	-	-	860	-	99.73
	46.31	52.85	3990	-	-	-	-	-	2020	-	-	-	-	-	99.80
	46.64	52.69	2420	-	-	-	-	-	890	180	-	-	-	-	99.73
	46.42	53.03	3350	220	540	-	1170	-	1880	-	-	-	-	-	100.18
	46.75	53.24	4200	300	-	-	-	570	1590	-	-	-	-	-	100.68
	47.70	52.82	5010	-	-	-	-	510	1810	110	-	600	-	-	101.34
	46.29	52.23	13290	-	-	-	-	3450	-	590	110	-	-	-	100.28
	46.15	52.39	3220	-	-	-	-	1760	520	1290	160	180	-	-	99.27
	46.05	52.69	2970	-	-	-	-	2410	470	950	-	-	-	-	99.44
	46.22	52.52	3730	-	-	-	-	2210	-	1650	310	-	-	-	99.54
	46.05	52.77	3530	-	-	-	-	1840	760	1280	-	220	-	-	99.59
	46.02	53.13	3550	-	-	-	-	4060	-	1470	-	-	-	-	100.07
	46.05	52.76	6570	-	-	-	-	4540	-	1330	-	-	-	-	100.10
	46.22	52.94	7740	-	1150	-	-	3110	-	1210	-	-	-	-	100.55
	45.51	52.61	9360	-	-	-	-	4450	-	1090	-	-	-	-	99.62
	46.14	52.96	6650	-	-	-	-	2650	670	830	470	-	-	-	100.23
	46.34	52.77	8230	-	-	-	-	2130	650	1380	-	-	-	-	100.35
	46.46	53.21	4280	-	-	-	-	-	500	810	130	-	-	-	100.28
	46.14	52.95	5380	-	-	-	-	-	-	940	-	-	430	950	-

4.5. Bulk Rock ICP OES Analyses

Preliminary bulk rock geochemical analyses were carried out on the mineralised samples (Table 3). Differences occurred between the two areas, concerning the As, Co, Cr, Ni, Zn, and Ag content.

Table 3. Results of bulk rock ICP OES analyses of the mineralised veins (- = below detection limit).

	As	Ag	Zn	Cu	Co	V	Cr	Ni
d.l. (ppm)	ppm	ppm	ppm	wt%	ppm	ppm	ppm	ppm
	50	10	25	25	50	25	25	25
Thirra	124,967	-	103	1.7	315	-	-	-
	272	18.3	3666	15.3	399	-	-	32.1
	1950	11.4	1944	14.2	1428	-	-	32.4
Kçira	-	-	129	22.8	130	52.3	168	98.5
	51.9	-	132	30.4	68.7	-	44.3	48.8

The Ag content of the Thirra deposit is between 10 and 20 mg/kg, while it is under 10 mg/kg in the samples from Kçira. Samples from Thirra have higher contents of As, Zn, and Co, while the ones from Kçira show higher Cr, Ni, V, and Cu.

5. Discussion

5.1. Metamorphic vs. Hydrothermal Alteration of the Host Rocks

According to the modal compositions of the host rocks, gabbro and gabbronorite occur at both deposits, which represents the mafic plutonic part of the oceanic lithosphere developed in the Neotethys Ocean. The majority of the analysed plagioclase laths show primary composition, as they are anorthite in Thirra, while anorthite and bytownite are present in Kçira (Figures 7 and 8). On the contrary, the plagioclase crystals with An_{12–59} composition are results of “Na-metasomatism”, as they are found in the vicinity of chlorite veins, indicating a circulating acidic and Si-rich fluid [31]. In addition, the circulating fluids could also cause the sericitisation of some plagioclase crystals. The apparent calcification of the plagioclase points to a later event caused by higher pH and Ca-enriched fluids.

Ca-poor but Mg-rich augite cores of the clinopyroxenes suggest a primary inhomogeneity of the mafic minerals, while in some cases Ca-loss can be detected at the rims, as a

result of a later fluid circulating event. Connected to this intense fluid circulation, the mafic minerals are often altered to chlorite and actinolite/tremolite, and the veins are filled with chlorite, epidote, prehnite, albite, and laumontite.

Chloritisation and uralitisation of the mafic minerals of the gabbroic rocks with the occurrence of epidote, prehnite, and chlorite indicate prehnite–actinolite metamorphic facies, thus a higher temperature subgreenschist alteration ($220\text{--}320\text{ }^{\circ}\text{C}$), and the lack of pumpellyite suggests a relatively low pressure with a maximum of 1.9 kbar [32]. In addition, the laumontite-bearing veins with chlorite, epidote, and prehnite that crosscut the samples, define the maximum pressure in 1.4 kbar and indicate a lower temperature event ($175\text{--}220\text{ }^{\circ}\text{C}$) (Figure 11). These values are in agreement with [21], who found that the maximum degree of metamorphism suffered by the Mirdita Zone rocks is lower greenschist facies.

In mafic rocks, minerals containing calcium, like prehnite, pumpellyite, epidote, actinolite, titanite, and calcite can form as a result of both magmatic hydrothermal processes and regional greenschist facies metamorphic events [33]. These processes can be separated based on the composition of epidote. The iron numbers of the analysed epidote grains are typical for the subgreenschist facies (Table 1, Figure 11), according to the calculations of [32]. However, we found several epidote crystals with low iron content (less than 10 wt% Fe_2O_3 and $\text{Fe}\# = 0.16 \pm 0.02$), which indicate a higher temperature than the subgreenschist facies, and rather high-temperature greenschist or amphibolite facies [32,33]. For the formation of epidote with such low Fe-contents, a higher metamorphic gradient is required, a depth of 7–8 km in the crust (calculating with an average $3.55\text{ }^{\circ}\text{C}/100\text{ m}$ thermal gradient) [34]. This contradiction can be resolved with a local heat flow resulting in higher temperature hydrothermal fluids, rather than the regional metamorphic grade of the region. Consequently, it is more likely that local subseafloor hydrothermal processes eventuated the mineralisations.

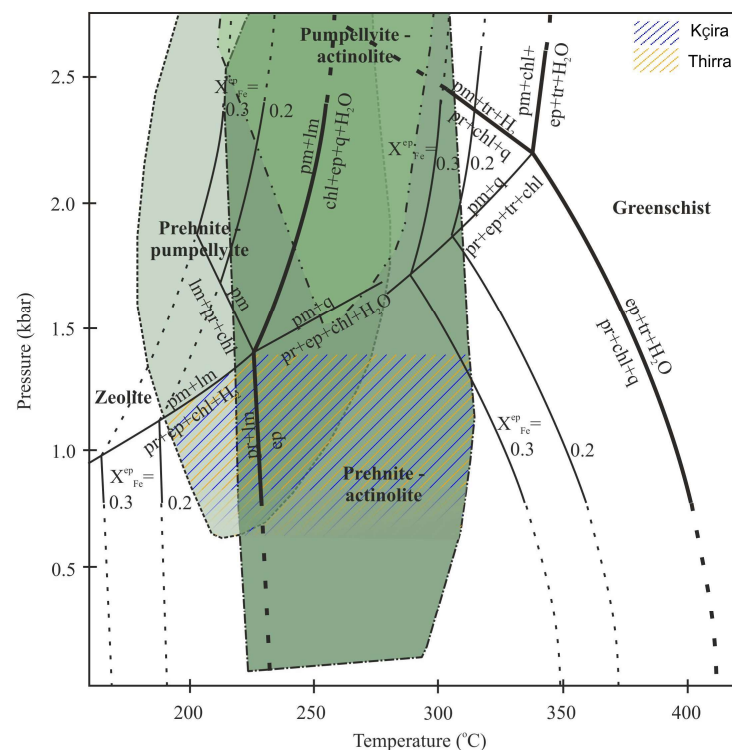


Figure 11. p-T diagram for the subgreenschist metamorphic facies; the estimated p-T ranges for the study areas are indicated. Thick lines indicate calculated borders of prehnite–pumpellyite, prehnite–actionolite, and pumpellyite–actionolite ranges after [32], while the green areas are based on the observations of [35] (after [36]). $X_{\text{ep}}^{\text{Fe}} = \text{Fe}^{3+}/(\text{Fe}^{3+} + \text{Al}^{3+})$.

Considering a hydrothermal origin, several papers evinced that Fe-rich epidote forms from cooler descending, while Fe-poor ones are from warmer ascending fluids (e.g., [37–42]). As most of the studied epidote grains are Fe-poor, the investigated deposits could have formed in an ancient hydrothermal system which was dominated by ascending fluids. In contrast, the few Fe-rich epidote grains occurring in some veins could form either during subgreenschist facies regional metamorphism or in a later stage of the hydrothermal event.

5.2. Fluid Parameters of the Ore Mineralisation and Deposit Type

A precipitation sequence of the Kçira deposit (Figure 12), based on the petrographic study, shows that the first minerals to precipitate are titanite, epidote, and chlorite—probably resulting from intense alteration of host rock clasts—defining a formation pressure of <1.6 kbar and temperature conditions between 175 and 320 °C (Figure 11). This p-T condition is supported by the appearance of the hydrothermal prehnite, which indicates a maximum pressure of 2 kbar and maximum temperature of 400 °C [32].

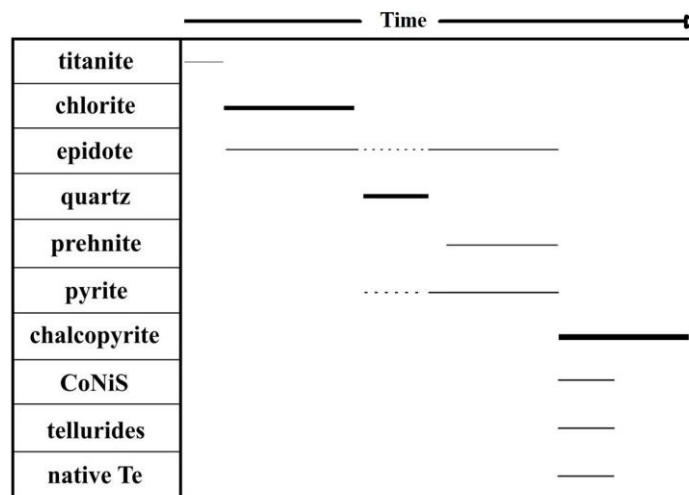


Figure 12. Observed precipitation sequence of the mineralised samples of Kçira. Line thickness refers to the quantity of the minerals in the samples, while dashed lines indicate uncertainties.

The first sulphide is pyrite, where the partly resorbed rims testify to a change in fluid parameters. Massive chalcopyrite with CoAs-sulphide, tellurides, and native tellurium represent the main ore-formation event in case of Kçira. The occurrence of Au Ag- and Ni-tellurides suggests very high f_{Te_2} , indicating mafic magmatic fluid addition (e.g., [43,44]), thus these minerals evince that the Kçira mineralisation formed from hydrothermal fluids associated with mafic magmatism.

In case of Thirra, the petrological observations indicate that the first minerals to precipitate are quartz and chalcopyrite; however, further chalcopyrite generations can also be observed in the pyrrhotite-chalcopyrite type mineralisation (Figure 13a). As the first stage of the ore mineralisation, sphalerite and pyrite accompanied chalcopyrite with minor cobaltite, and then co-precipitating pyrrhotite and chalcopyrite superimposed the earlier minerals. The formation temperature of sphalerite is usually less than 250 °C, and it precipitates in either the earliest or the latest stage of a hydrothermal activity, while the chalcopyrite usually crystallises at higher temperatures, around 280–320 °C [45,46]. The occurring chalcopyrite disease in cases of the studied sphalerite indicates a change in the ore-forming fluid parameters, as higher temperature, higher f_{S_2} , and Cu-rich fluid causes Cu diffusion after the precipitation of the sphalerite [47,48]. Change of the fluid parameters can also be observed as the formation of cobaltite grains is followed by chalcopyrite (Figure 10d). Cobaltite forms at high temperatures in hydrothermal environments [49–51], thus this phenomenon may indicate a decrease in temperature. Repeated mineral precipitation events can be detected in the samples, e.g., quartz, pyrite, and chalcopyrite appear in several

generations. The observed Fe-oxides/hydroxides pseudomorphs after pyrite indicate an oxidative environment after the hydrothermal process.

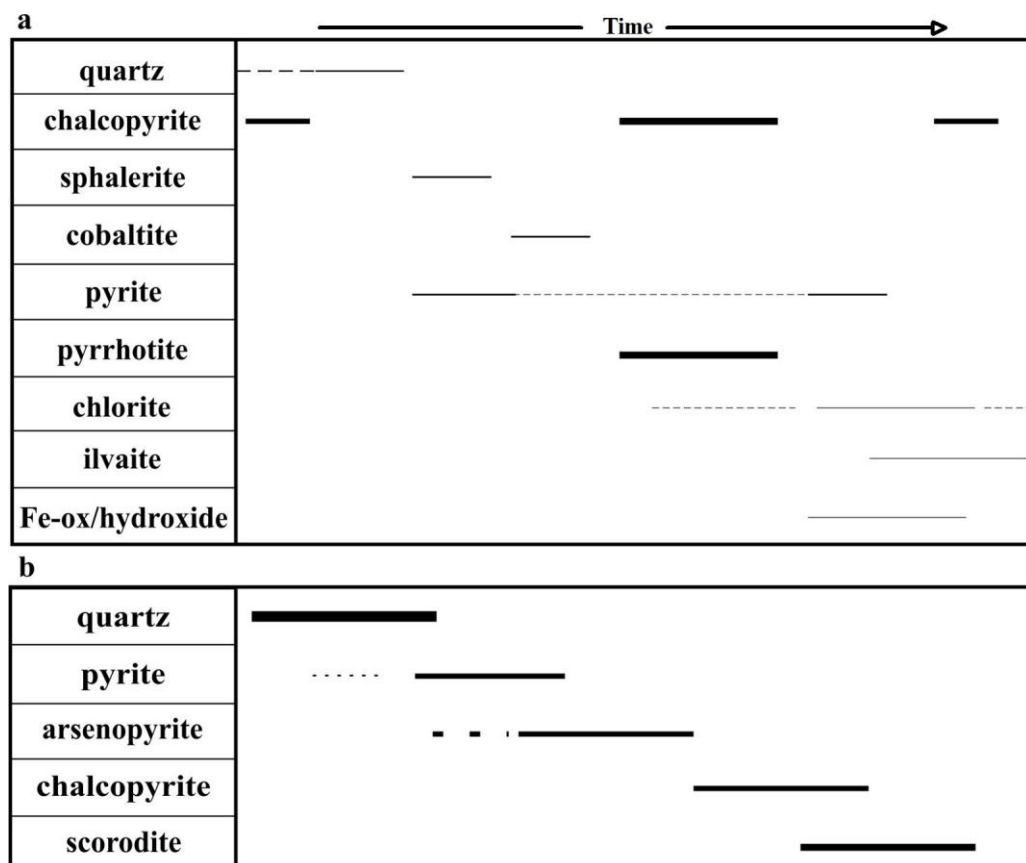


Figure 13. Observed precipitation sequences of the pyrrhotite-chalcopyrite type (a) and the chalcopyrite-arsenopyrite-pyrite type mineralisations (b) of Thirra. Line thickness refers to the quantity of the minerals in the samples, while dashed lines indicate uncertainty.

Arsenopyrite occurs as the cement-between-quartz clasts and as pyrite pseudomorphs in the chalcopyrite-arsenopyrite-pyrite type mineralisation (Figure 13b). Chalcopyrite precipitated in more generations: one is right after the arsenopyrite, while another occurs in the veins. The formation of scorodite is the result of the latest stage of mineralisation, where the oxidation of the arsenopyrite took place thanks to an oxidative and low pH fluid.

Differences are observable concerning the mineralogical compositions of the two deposits: at Thirra, arsenopyrite, scorodite, and sphalerite occur, while these are missing at Kçira. The explanation can be found in the geochemical affinity (i.e., compatibility) of Zn and As. The aforementioned minerals formed in an SSZ area, where the magmatic rocks of the crust are enriched in incompatible elements [21]. It is known from [52] that As is one of the first elements which leaves the slab and enters the mantle wedge. The same is true for Zn, as it is also an incompatible element, thus it is more likely that sphalerite appears in an SSZ than in an MOR area.

Due to the lack of recrystallisation and the only low-grade metamorphic processes affecting the region, the chemical composition of the sulphides—considered together with the texture and paragenesis—are informative for the ore-forming processes and fluids [53–55]. We used the mineral chemistry of pyrite to draw further conclusions about the formation conditions of the mineralisations.

The chemical composition of pyrite grains provides information about the origin of their parental fluids: magmatic, hydrothermal, seawater and freshwater origins are distinguishable based on the trace elements and especially their Co:Ni ratios [56–62]. Our Co vs. Ni results are similar to the literature data of stockwork zones of VMS deposits

(Figure 14a); therefore, this supports the conclusions drawn from the mineral paragenesis. This finding is also in comparison with the results of [63], who were able to discriminate the sulphides of the stockwork zone from the stratabound massive lens based on the Co and Ni contents of pyrite grains in the VMS deposit of Skouriotissa, Cyprus (Figure 14b).

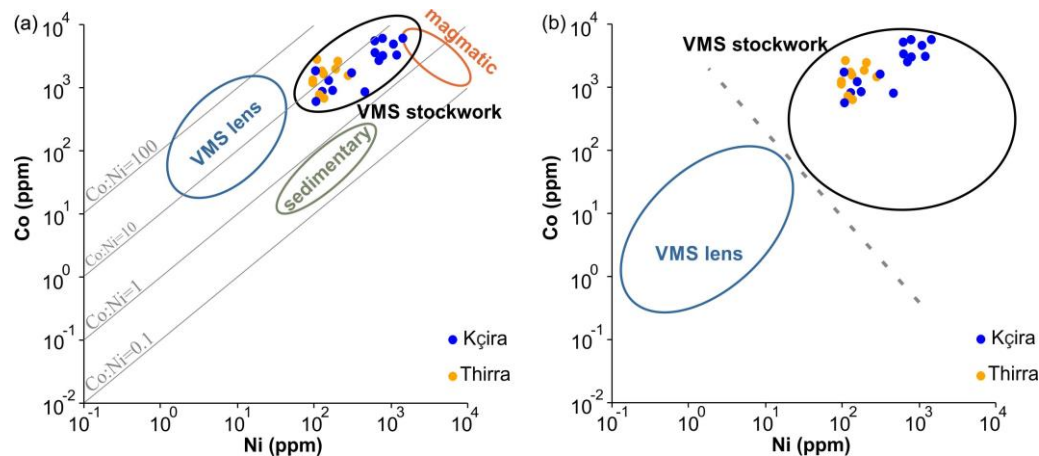


Figure 14. Co and Ni contents of the analysed pyrite grains. (a) Our results compared to characteristic values of pyrites from different geological environments (the fields are drawn based on [64,65]). (b) Our results compared to the data of [63].

It is generally accepted that the rocks in which the hydrothermal fluids circulate affect the hydrothermal mineralisations; thus, there is a strong connection between the compositions of the host rocks and the minerals precipitated from the fluids [10,11]. The investigated deposits occur in gabbro and gabbronorite; however, significant differences were observed between the two areas concerning the concentrations and ratios of the Co and Ni of the pyrites (Table 2, Figure 14). Generally, the concentrations and ratios of these highly compatible elements are higher in the MOR area (Kçira) compared to the SSZ one (Thirra).

Ref. [63] compares the Ni-, Co-, Se-, and Te concentrations with the Fe-content of pyrite, which can also be used to make distinctions between the VMS lens and the stockwork zone; in addition, the stockwork part can be divided into a shallow and deep stockwork zone based on the Se contents (Figure 15c). Our pyrite grains show trace element contents similar to VMS stockwork deposits; furthermore, the Se vs. Fe diagram indicates that the samples formed in the deep stockwork zone (Figure 15).

Extremely high concentrations of Co occur in some pyrite grains (up to 5900 ppm), indicating a high-temperature fluid present where the role of seawater was subordinate [66]. The elevated concentration of Cu (1.3 wt%) also points to a high-temperature fluid, because a mixing with cold seawater would cool the system leading to chalcopyrite precipitation—with a significant Co-content; therefore, the pyrite would be Cu- and Co-poor [67].

The bulk rock geochemical compositions of the analysed rocks correlate well with the differences apparent in the mineralogical compositions between the two areas. The copper mineralisation of the SSZ-like Eastern-type ophiolite belt is enriched in strongly incompatible elements (As, Zn), while the concentrations of compatible elements (V, Cr, Ni) are significantly lower compared to the MOR-like Western-type ophiolite belt (Table 3). The Cu—unlike Pb, Zn, and Ag—is enriched in mafic rocks of MOR environments [68], and thus the circulating fluids can be enriched in Cu in these environments.

Based on the concentrations of three common base metals (Cu, Zn and Pb), the investigated deposits are Cu-type VMS deposits [69,70], while considering the type of host rocks—which is also indicative of the geotectonic situation—these are mafic = Cyprus-type VMS deposits [11] (Figure 16).

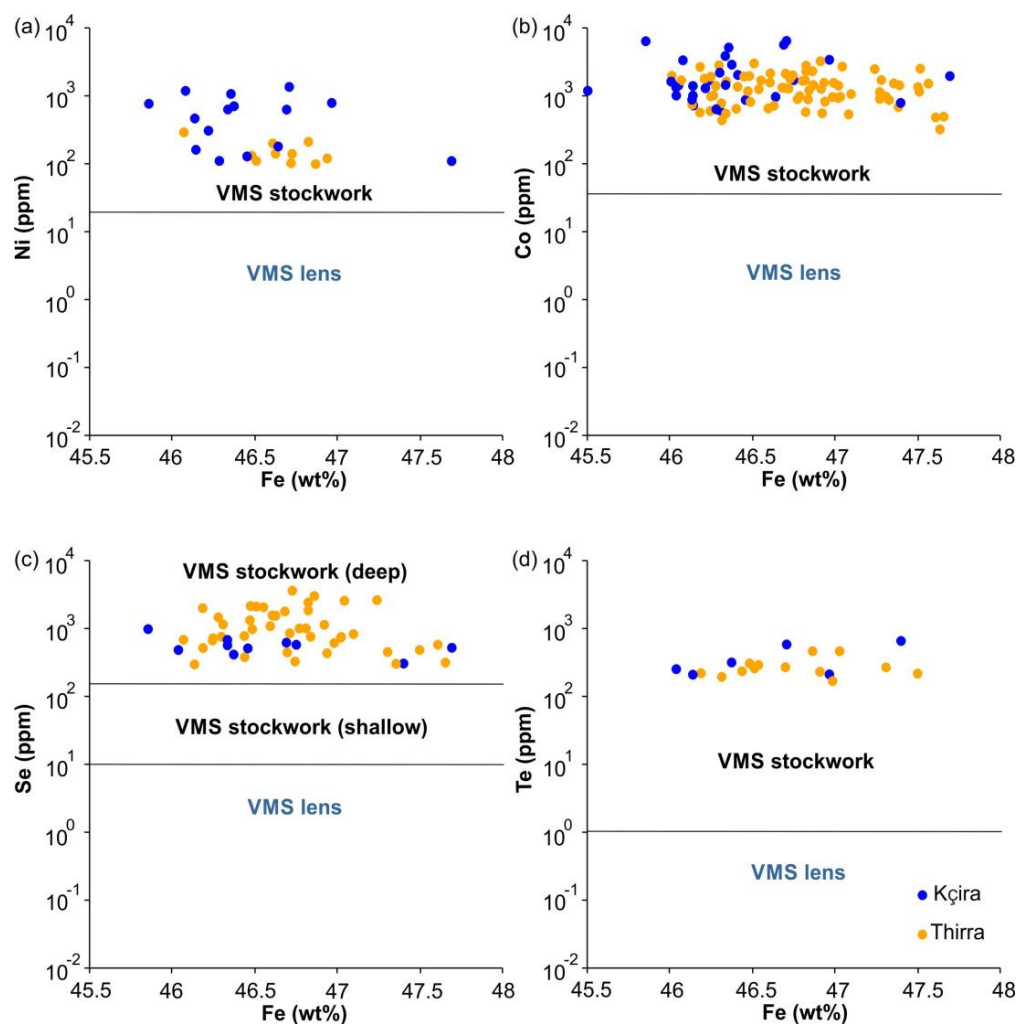


Figure 15. Trace elements and iron content diagrams of the analysed pyrite grains: (a) Ni vs. Fe; (b) Co vs. Fe; (c) Se vs. Fe; and (d) Te vs. Fe contents. The fields are divided based on [63].

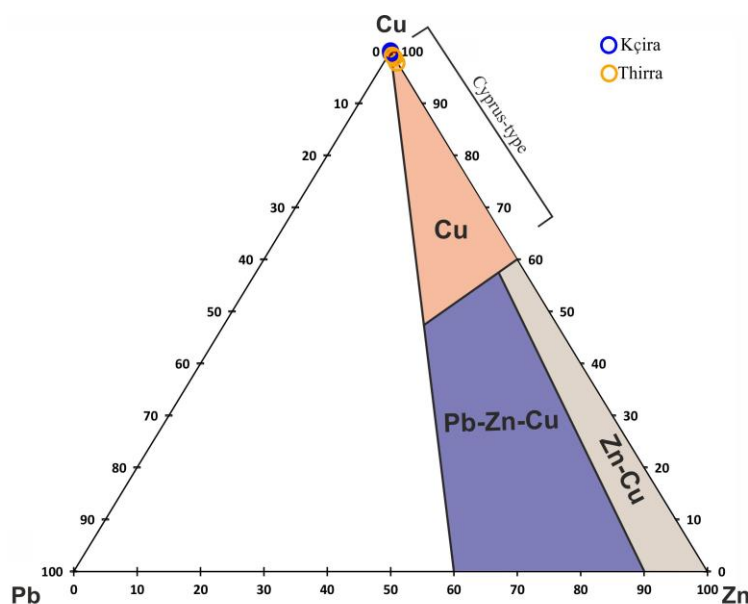


Figure 16. The analysed bulk samples are shown on the Cu-Zn-Pb triangle diagram, with the Cyprus-type VMS field indicated (based on [11,70]).

6. Conclusions

- The two investigated copper deposits of the Albanian Mirdita Zone are hosted in strongly altered gabbro and gabbronorite.
- A local high-temperature hydrothermal fluid flow is indicated, as the alteration reached a higher temperature than the known metamorphism.
- The samples from the western Kçira are richer in compatible elements, while those from the eastern Thirra have higher concentrations of incompatible elements, reflecting their original geodynamic settings (MOR and SSZ, respectively).
- So far, unknown minerals have been identified in the deposits: ilvaite, scorodite, Ni- and AgAu-tellurides, native tellurium, and prehnite.
- Based on the trace element contents of the pyrite grains (Co, Ni, Te, Se) and the mineral chemical composition of the epidote, the deposits are identified as the deep stockwork feeder zones of VMS systems.

Consequently, the Kçira and Thirra deposits are mafic-, Cyprus-, and thus Cu-type VMS mineralisations, representing the feeder zone of the hydrothermal system, with the detected mineralogical and geochemical differences related to their different geotectonic situations. Further evaluations for the ore potential of these deposits are needed in the future, as well as fluid inclusion and stable isotope geochemical studies (H, O, S, Cu, Fe).

Author Contributions: Conceptualization, A.V.-L.; methodology, A.V.-L. and G.B.K.; formal analysis, A.V.-L. and Z.K.; investigation, A.V.-L. and Z.K.; resources, A.V.-L.; writing—original draft preparation, A.V.-L.; writing—review and editing, Z.K. and G.B.K.; visualization, A.V.-L.; supervision, G.B.K.; funding acquisition, A.V.-L. and G.B.K. All authors have read and agreed to the published version of the manuscript.

Funding: The research was supported by the ÚNKP-16-2 New National Excellence Program of the Ministry of Human Capacities (to A.V.-L.), and the OTKA, PD 112580 by NKFIH (to G.B.K.). The work of G.B.K. is partly supported by the János Bolyai Research Scholarship awarded by the Hungarian Academy of Sciences and the ÚNKP-23-5 New National Excellence Program of the Ministry for Culture and Innovation from the source of the National Research, Development and Innovation Fund.

Data Availability Statement: The raw data supporting the conclusions of this article will be made available by the authors on request.

Acknowledgments: Gjon Kaza, Tonin Deda and Donald Deda are thanked for their selfless help with the sampling in 2016. The University Centrum of Applied Geosciences (UCAG) is thanked for the access to the E. F. Stumpfl Electron Microprobe Laboratory, Leoben. The authors are grateful to Federica Zaccarini for providing the EPMA analyses.

Conflicts of Interest: The authors declare no conflicts of interest. The funders had no role in the design of the study; in the collection, analyses, or interpretation of data; in the writing of the manuscript, or in the decision to publish the results.

References

1. Hoxha, L.; Scott, P.W.; Eyre, M. The geological setting of volcanogenic sulphide orebodies in Albanian ophiolites. *Appl. Earth Sci.* **2005**, *114*, 33–52. [[CrossRef](#)]
2. Milushi, I.; Jata, I.; Vukzaj, N.; Gjeci, K. Exploration Complex Methods of Copper Ore in the Volcano-sedimentary Formation of Porave Area, Puka. In Proceedings of the 7th Congress of the Balkan Geophysical Society, EAGE Publications, Tirana, Albania, 7–10 October 2013. [[CrossRef](#)]
3. Doda, V.; Deda, D.; Alliu, I. Sulphide mineralization in gabbro and plagiogranites in Ophiolites of Albanides. In Proceedings of the XX CBGA Congress, Tirana, Albania, 24–26 September 2014.
4. Bele, S.; Kamberaj, R. The ore deposit 3D modelling, new effective solution in the optimization of geological and mining works. *Earth Sci.* **2017**, *6*, 35–43.
5. Kaza, G.; Doda, V.; Naco, P.; Onuzi, K.; Gjeci, K.; Vincani, F.; Gjonaj, V. Geological-structural setting of massif and the levels of quartz-sulphide mineralization in the Kaptina Gabbro Massif. *Int. J. Eng. Res. Appl.* **2014**, *4*, 1–11.

6. Dubé, B.; Gosselin, P. Greenstone-hosted quartz-carbonate vein deposits. In *Mineral Deposits of Canada: A Synthesis of Major Deposit-Types, District Metallogeny, the Evolution of Geological Provinces, and Exploration Methods*; Goodfellow, W.D., Ed.; Special Publication; Geological Association of Canada, Mineral Deposits Division: St. John's, NF, Canada, 2007; pp. 49–73.
7. Cox, S.F.; Etheridge, M.A.; Wall, V.J. The role of fluids in syntectonic mass transport, and the localization of metamorphic vein-type ore deposits. *Ore Geol. Rev.* **1986**, *2*, 65–86. [\[CrossRef\]](#)
8. Hurai, V.; Lexa, O.; Schulmann, K.; Montigny, R.; Prochaska, W.; Frank, W.; Konecny, P.; Ioannou, S.E.; Spooner, E.T.C.; Barrie, C.T. Fluid temperature and salinity characteristics of the Matagami volcanogenic massive sulfide district. Quebec. *Econ. Geol.* **2007**, *102*, 691–715.
9. N'diaye, I.; Essaifi, A.; Dubois, M.; Lacroix, B.; Goodenough, K.M.; Maacha, L. Fluid flow and polymetallic sulfide mineralization in the Kettara shear zone (Jebilet Massif, Variscan Belt, Morocco). *J. Afr. Earth Sci.* **2016**, *119*, 17–37. [\[CrossRef\]](#)
10. Zaccarini, F.; Garuti, G. Mineralogy and chemical composition of VMS deposits of northern Apennine ophiolites, Italy: Evidence for the influence of country rock type on ore composition. *Miner. Petrol.* **2008**, *94*, 61–83. [\[CrossRef\]](#)
11. Barrie, C.T.; Hannington, M.D. Introduction: Classification of VMS deposits based on host rock composition. In *Volcanic-Associated Massive Sulfide Deposits: Processes and Examples in Modern and Ancient Settings*; Barrie, C.T., Hannington, M.D., Eds.; Society of Economic Geology: Littleton, CO, USA, 1999; Volume 8, pp. 2–10.
12. Robertson, A.H.F.; Dixon, J.E. Introduction: Aspects of the geological evolution of the Eastern Mediterranean. In *The Geological Evolution of the Eastern Mediterranean*; Dixon, J.E., Robertson, A.H.F., Eds.; Geological Society London Special Publication 17; Geological Society: London, UK, 1984; pp. 591–602.
13. Robertson, A.H.F.; Shallo, M. Mesozoic-Tertiary tectonic evolution of Albania in its regional Eastern Mediterranean context. *Tectonophysics* **2000**, *316*, 197–254. [\[CrossRef\]](#)
14. Zelic, M.; Agostini, S.; Marroni, M.; Pandolfi, L.; Tonarini, S. Geological and Geochemical Features Of The Kopaonik Intrusive Complex (Vardar Zone, Serbia). *Ophioliti* **2010**, *35*, 33–47.
15. Hoxha, M.; Boullier, A. The peridotites of the Kukes ophiolite (Albania): Structure and kinematics. *Tectonophysics* **1995**, *249*, 217–231. [\[CrossRef\]](#)
16. Bortolotti, V.; Kodra, A.; Marroni, M.; Mustafa, F.; Pandolfi, L.; Principi, G.; Saccani, E. Geology and petrology of ophiolitic sequences in the Mirdita region (Northern Albania). *Ophioliti* **1996**, *21*, 3–20.
17. Shallo, M.; Dilek, Y. Development of the ideas on the origin of Albanian ophiolites. In *Special Paper 373: Ophiolite Concept and the Evolution of Geological Thought*; Geological Society of America: Boulder, CO, USA, 2003; pp. 351–363. [\[CrossRef\]](#)
18. Dilek, Y.; Furnes, H. Structure and geochemistry of Tethyan ophiolites and their petrogenesis in subduction rollback systems. *Lithos* **2009**, *113*, 1–20. [\[CrossRef\]](#)
19. Dimo-Lahitte, A.; Monie, P.; Vergely, P. Metamorphic soles from the Albanian ophiolites: Petrology, $^{40}\text{Ar}/^{39}\text{Ar}$ geochronology, and geodynamic evolution. *Tectonics* **2001**, *20*, 78–96. [\[CrossRef\]](#)
20. Dilek, Y.; Furnes, H.; Shallo, M.; Mortensen, J.K. Structure, petrology, and geochronology of the Albanian ophiolites and their tectonic evolution within the Neotethyan orogenic belt, In, EUG XI, European Union of Geosciences, Strasbourg, France. *J. Conf. Abstr.* **2001**, *6*, 321.
21. Dilek, Y.; Furnes, H.; Shallo, M. Geochemistry of the Jurassic Mirdita Ophiolite (Albania) and the MORB to SSZ evolution of a marginal basin oceanic crust. *Lithos* **2008**, *100*, 174–209. [\[CrossRef\]](#)
22. Marcucci, M.; Kodra, A.; Pirdeni, A.; Gjata, T. Radiolarian assemblage in the Triassic and Jurassic cherts of Albania. *Ophioliti* **1994**, *19*, 110–114.
23. Marcucci, M.; Prela, M. The Lumi i Zi (Puke) section of the Kalur Cherts: Radiolarian assemblages and comparisons with other sections in northern Albania. *Ophioliti* **1996**, *21*, 71–77.
24. Robertson, A.; Ionescu, C.; Hoeck, V.; Koller, F.; Onuzi, K.; Bucur, I.; Ghega, D. Emplacement of the Jurassic Mirdita ophiolites (southern Albania): Evidence from associated clastic and carbonate sediments. *Int. J. Earth Sci.* **2012**, *101*, 1535–1558. [\[CrossRef\]](#)
25. Cortesogno, L.; Gaggero, L.; Jaho, E.; Marroni, M.; Pandolfi, L.; Shtjefanaku, D. The gabbroic complex os the Western Ophiolitic Belt, Northern Albania: An example of multilayered sequence in an intermediete-spreading oceanic ridge. *Ophioliti* **1998**, *2*, 49–64.
26. Xhomo, A.; Kodra, A.; Dimo, L.L.; Xhafa, Z.; Nazaj, S.H.; Nakuci, V.; Yizeraj, D.; Lula, F.; Sadushi, P.; Shallo, M.; et al. *Geological Map of Albania, M = 1:200 000*; Albanian Geological Survey: Tirana, Albania, 2002.
27. Kaza, G.; Beqiraj, A.; Gjonaj, V.; Doda, V.; Ormeni, R. Structural and Mineralogical Features of the Quartz Sulphur Mineralization from the Gabbroic Massif of Kaptena (Mirdita Ophiolitic Complex of Albania). *Int. J. Eng. Res. Appl.* **2012**, *7*, 170–177.
28. Morimoto, N.; Fabries, J.; Ferguson, A.K.; Ginzburg, I.V.; Ross, M.; Seifert, F.A.; Zussman, J. Nomenclature of pyroxenes. *Am. Min.* **1988**, *73*, 1123–1133.
29. Deer, A.W.; Howie, R.A.; Zussman, J. *Rock-Forming Minerals 4*; Wiley: New York, NY, USA, 1963.
30. Friedl, J.; Wagner, F.E.; Wang, N. On the chemical state of combined gold in sulfidic ores: Conclusions from Mössbauer source experiments. *Neues Jahrb. Mineral. Abh.* **1995**, *169*, 279–290.
31. Seyfried, W. Experimental and theoretical constraints on hydrothermal alteration processes at mid-ocean ridges. *Ann. Rev. Earth Planet. Sci. Lett* **1987**, *15*, 317–335. [\[CrossRef\]](#)
32. Liou, J.; Maruyama, S.; Cho, M. Phase Equilibria and mineral parageneses of metabasites in low-grade metamorphism. *Mineral. Mag.* **1985**, *49*, 321–333. [\[CrossRef\]](#)

33. Hannington, M.D.; Santaguida, F.; Kjarsgaard, I.M.; Cathles, L.M. Regional-scale hydrothermal alteration in the Central Blake River Group, western Abitibi subprovince, Canada: Implications for VMS prospectivity. *Miner. Depos.* **2003**, *38*, 393–422. [[CrossRef](#)]
34. Powell, W.G.; Carmichael, D.M.; Hodgson, C.J. Conditions and timing of metamorphism in the southern Abitibi greenstone belt, Quebec. *Can. J. Earth Sci.* **1995**, *32*, 787–805. [[CrossRef](#)]
35. Frey, M.; De Capitani, C.; Liou, J. A new petrogenetic grid for low-grade metabasites. *J. Metam. Geol.* **1991**, *9*, 497–509. [[CrossRef](#)]
36. Skoda, P. Vulkanogén Masszív Szulfid Telepek Stockwork Zónájának Fluidzárvány Vizsgálata Casali-Monte Loreto Térségében (Északi-Appenninek, Olaszország). Master’s Thesis, Eötvös Loránd University, Budapest, Hungary, 2017.
37. Stakes, D.S.; O’Neil, J.R. Mineralogy and stable isotope geochemistry of hydrothermally altered oceanic rocks. *Earth Planet. Sci. Lett.* **1982**, *57*, 285–304. [[CrossRef](#)]
38. Alt, J.C.; Muehlenbachs, K.; Honnorez, J. An oxygen isotopic profile through the upper kilometer of the oceanic crust. DSDP Hole 504B. *Earth Planet. Sci. Lett.* **1986**, *80*, 217–229. [[CrossRef](#)]
39. Delaney, J.R.; Mogk, D.M.; Mottl, M.J. Quartz-cemented breccias from the Mid-Atlantic Ridge: Samples of a high salinity upflow zone. *J. Geophys. Res.* **1987**, *92*, 9175–9192. [[CrossRef](#)]
40. Gillis, K.M.; Robinson, P.T. Distribution of alteration zones in the upper oceanic crust. *Geology* **1988**, *16*, 262–266. [[CrossRef](#)]
41. Bettison, L. Petrogenetic Studies of Epidotes and Mixed-Layer Chlorite/Smectite in Submarine Hydrothermal Systems. Ph.D. Thesis, University of California, Davis, CA, USA, 1991.
42. Gillis, K.M.; Thompson, G. Metabasalts from the Mid-Atlantic Ridge: New insights into hydrothermal systems in slow-spreading crust. *Contrib. Mineral. Petrol.* **1993**, *113*, 502–523. [[CrossRef](#)]
43. Afifi, A.M.; Kelly, W.C. Phase relations among tellurides, sulfides, and oxides; Pt. II, Applications to telluride-bearing ore deposits. *Econ. Geol.* **1988**, *83*, 395–404. [[CrossRef](#)]
44. Hassan, L.Y.; Roberts, M.P. Tellurides associated with volcanogenic massive sulfide (VMS) mineralization at Yuinmery and Austin, Western Australia. *Ore Geol. Rev.* **2017**, *80*, 352–362. [[CrossRef](#)]
45. Ohmoto, H. Formation of volcanogenic massive sulphide deposits: The Kuroko perspective. *Ore Geol. Rev.* **1996**, *10*, 135–177. [[CrossRef](#)]
46. Hannington, M.D.; de Ronde, C.E.J.; Petersen, S. Modern sea-floor tectonics and submarine hydrothermal systems. *Econ. Geol.* **2005**, *100*, 111–141.
47. Bortnikov, N.S.; Genkin, A.D.; Dobrovolskaya, M.G.; Muravitskaya, G.N.; Filimonova, A.A. The nature of chalcopyrite inclusions in sphalerite: Exsolution, coprecipitation, or “disease”? *Econ. Geol.* **1991**, *86*, 1070–1082. [[CrossRef](#)]
48. Bente, K.; Doering, T. Experimental studies on the solid state diffusion of Cu + In in ZnS and on “Disease”, DIS (Diffusion Induced Segregations), in sphalerite and their geological applications. *Miner. Petrol.* **1995**, *53*, 285–305. [[CrossRef](#)]
49. Ramdohr, P.; Cobaltite. *The Ore Minerals and their Intergrowths*; Ramdohr, P., Ed.; Pergamon Press: Braunschweig, Germany, 1969; pp. 814–820.
50. Klein, C. *Manual of Mineralogy*, 22nd ed.; John Wiley & Sons Inc.: Hoboken, NJ, USA, 2002; pp. 333–370.
51. Haldar, S.K. *Platinum-Nickel-Chromium Deposits*; Elsevier: Amsterdam, The Netherlands, 2017; pp. 1–34.
52. Noll, P.D.; Newsom, H.E.; Leeman, W.P.; Ryan, J.G. The role of hydrothermal fluids in the production of subduction zone magmas: Evidence from siderophile and chalcophile trace elements and boron. *Geochim. Cosmochim. Acta* **1996**, *60*, 587–611. [[CrossRef](#)]
53. Abraitis, P.K.; Patrck, R.A.D.; Vaughan, D.J. Variations in the compositional, textural and electrical properties of natural pyrite: A review. *Int. J. Miner. Process.* **2004**, *74*, 41–59. [[CrossRef](#)]
54. Reich, M.; Deditius, A.; Chryssoulis, S.; Li, J.-W.; Ma, C.-Q.; Parada, F.; Barra, P.F.; Mittermayr, F. Pyrite as a record of hydrothermal fluid evolution in a porphyry copper system: A SIMS/EMPA trace element study. *Geochim. Cosmochim. Acta* **2013**, *104*, 42–62. [[CrossRef](#)]
55. Genna, D.; Gaboury, D. Deciphering the hydrothermal evolution of a VMS System by LA-ICP-MS using trace elements in pyrite: An example from the Bracemac- McLeod Deposits, Abitibi, Canada, and implications for exploration. *Econ. Geol.* **2015**, *110*, 2087–2108. [[CrossRef](#)]
56. Carstens, C.W. Om geokjemiske undersøkelser av malmer. *Norsk Geol. Tidsskr.* **1941**, *21*, 213–221.
57. Hegemann, F. Die geochemische Bedeutung von Kobalt und Nickel im Pyrit. *Z. Angew. Mineral.* **1943**, *4*, 122–239.
58. Hegemann, F. Die geochemisehe Bedeutung Von Kobalt und Nikel in Pyrit. *Z. Angew. Mineral.* **1943**, *4*, 2–3.
59. Gavelin, S.; Gabrielson, O. Spectrochemical investigation of sulphide minerals from the ores of the Skellefte district. *Sveriges Geologiska Undersökning* **1947**, *41*, 1–45.
60. Hawley, J.E.; Nichol, I. Trace elements in pyrite, pyrrhotite and chalcopyrite of different ores. *Econ. Geol.* **1961**, *56*, 467–487. [[CrossRef](#)]
61. Bralia, A.; Sabatini, G.; Troja, F. A revaluation of the Co/Ni ratio in pyrite: A geochemical tool in ore genesis problems. *Miner. Depos.* **1979**, *14*, 353–374. [[CrossRef](#)]
62. Mookherjee, A.; Philip, R. Distribution of copper, cobalt and nickel in ores and host-rocks, Ingladhal, Karnataka, India. *Miner. Depos.* **1979**, *14*, 33–55. [[CrossRef](#)]
63. Keith, M.; Haase, K.M.; Klemd, R.; Kruss, S.; Strauss, H. Systematic variations of trace element and sulfur isotope compositions in pyrite with stratigraphic depth in the Skouriotissa volcanic-hosted massive sulfide deposit, Troodos ophiolite, Cyprus. *Chem. Geol.* **2016**, *423*, 7–18. [[CrossRef](#)]

64. Bajwah, Z.U.; Seccombe, P.K.; Offler, R. Trace element distribution, Co: Ni ratios and genesis of the Big Cadia iron-copper deposit, New South Wales, Australia. *Miner. Depos.* **1987**, *22*, 292–300. [[CrossRef](#)]
65. Song, X. Minor Elements and Ore Genesis of the Fankou Lead-Zinc Deposit, China. *Miner. Depos.* **1984**, *19*, 95–104.
66. Huston, D.L.; Sie, S.H.; Suter, G.F.; Cook, D.R.; Both, R.A. Trace Elements in Sulfide Minerals from Eastern Australian Volcanic-Hosted Massive Sulfide Deposits Part I. Proton Microprobe analyses of Pyrite, Chalcopyrite and Sphalerite and Part II. Selenium Levels in Pyrite: Comparison with $\delta^{34}\text{S}$ values and Implications for the Source of Sulfur in Volcanogenic hydrothermal Systems. *Econ. Geol.* **1995**, *90*, 1167–1196.
67. Keith, M.; Häckel, F.; Haase, K.M.; Schwarz-Schampera, U.; Klemd, R. Trace element systematics of pyrite from submarine hydrothermal vents. *Ore Geol. Rev.* **2016**, *72*, 728–745. [[CrossRef](#)]
68. Levinson, A.A. *Introduction to Exploration Geochemistry*; Applied Publishing Ltd.: Calgary, AB, Canada, 1974; p. 612.
69. Lydon, J.W. Volcanogenic massive sulfide deposits, Part 2: Genetic models. *Geosci. Can.* **1988**, *15*, 155–181.
70. Large, R.R. Australian volcanic-hosted massive sulfide deposits: Features, styles and genetic models. *Econ. Geol.* **1992**, *87*, 471–510. [[CrossRef](#)]

Disclaimer/Publisher’s Note: The statements, opinions and data contained in all publications are solely those of the individual author(s) and contributor(s) and not of MDPI and/or the editor(s). MDPI and/or the editor(s) disclaim responsibility for any injury to people or property resulting from any ideas, methods, instructions or products referred to in the content.